AGU ADVANCING EARTH AND SPACE SCIENCES

JGR Biogeosciences

RESEARCH ARTICLE
10.1029/2024JG008581

Magnitude Shifts in Aeolian Sediment Transport Associated With Degradation and Restoration Thresholds in Drylands

Nicholas P. Webb[1], Brandi Wheeler[1], Brandon L. Edwards[1], Jeremy W. Schallner[1], Neeshia Macanowicz[2], Justin W. Van Zee[1], Ericha M. Courtright[1], Brad Cooper[1], Sarah E. McCord[1], Dawn Browning[1], Saroj Dhital[1], Kristina E. Young[1], and Brandon T. Bestelmeyer[1]

[1]USDA-ARS Jornada Experimental Range, Las Cruces, NM, USA, [2]Department of Biology, New Mexico State University, Las Cruces, NM, USA

Key Points:

- Aeolian sediment transport rates changed over four orders of magnitude across grassland to shrubland ecological states
- Critical perennial grass cover thresholds for magnitude shifts in transport rates were associated with ecological state transitions
- Results suggest that ecological state is a primary control on aeolian sediment transport and dust emissions from vegetated drylands

Supporting Information:

Supporting Information may be found in the online version of this article.

Correspondence to:

N. P. Webb,
Nick.Webb@usda.gov

Citation:

Webb, N. P., Wheeler, B., Edwards, B. L., Schallner, J. W., Macanowicz, N., Van Zee, J. W., et al. (2025). Magnitude shifts in aeolian sediment transport associated with degradation and restoration thresholds in drylands. *Journal of Geophysical Research: Biogeosciences*, *130*, e2024JG008581. https://doi.org/10.1029/2024JG008581

Received 2 NOV 2024
Accepted 22 FEB 2025

Author Contributions:

Conceptualization: Nicholas P. Webb, Brandi Wheeler, Neeshia Macanowicz, Justin W. Van Zee, Dawn Browning, Brandon T. Bestelmeyer
Data curation: Brandi Wheeler, Neeshia Macanowicz, Justin W. Van Zee, Ericha M. Courtright, Brad Cooper, Sarah E. McCord
Formal analysis: Nicholas P. Webb, Brandi Wheeler, Brandon L. Edwards, Jeremy W. Schallner

Abstract Vegetation change in drylands can influence wind erosion and sand and dust storms (SDS) with far-reaching consequences for Earth systems and society. Although vegetation is recognized as an important control on wind erosion and SDS, the interactions are not well described at the landscape level or in the context of dryland ecosystem change. The transition of sites from one ecological state to another (e.g., grassland to shrubland) is typically associated with changes in the composition, cover, and structure of vegetation, which influence drag partitioning and wind shear velocities that drive aeolian sediment transport. Here, we quantify the magnitude and direction of aeolian sediment transport responses to ecological state change in the northern Chihuahuan Desert and identify thresholds associated with state transitions. Our results show aeolian sediment mass flux (Q) increased from ~1 to 10 g m^{-1} d^{-1} in historical grassland with scattered shrubs to ~10–100 g m^{-1} d^{-1} following shrub invasion and decline in perennial grass cover to ~100–10,000 g m^{-1} d^{-1} in shrubland following complete grass loss. The magnitude shifts were associated with critical perennial grass cover thresholds governing nonlinear increases in Q across ecological state transitions. Grass recovery in shrubland reduced Q to rates similar to those in historical grasslands—a multiple order of magnitude reduction. Our results show that crossing degradation and restoration thresholds between alternative ecological states can have a profound effect on the magnitude and spatiotemporal variability of aeolian sediment transport and primacy in determining patterns of wind erosion and dust emissions in vegetated drylands.

Plain Language Summary In this study, we investigate how dryland vegetation change can influence wind-driven sediment transport. We use measurements of vegetation composition, cover, and structure (height and spacing) collected in the northern Chihuahuan Desert to understand change in sediment transport by wind in different ecological states, representing historical grassland and alternative vegetation communities that have resulted from shrub invasion and degradation and restoration processes that affect grass cover. Our results show over four orders of magnitude change in sediment transport rates following a trajectory of degradation and a decrease in sediment transport rates over the same range in response to grass recovery. Sediment transport rates were highly sensitive to degradation and recovery thresholds between alternative ecological states, suggesting that patterns of wind erosion in vegetated drylands are likely determined by patterns of vegetation disturbance and recovery that are often unique to different soil types and landscape settings.

1. Introduction

Dryland soils and plant communities are changing globally in response to pervasive stressors of drought, climate change, invasive species, changing disturbance regimes, and management (Mirzabaev et al., 2019). Changes in vegetation composition, cover, and structure (height and spatial arrangement) associated with land degradation have the potential to increase wind and water erosion, which may lead to permanent loss of ecosystem services (Webb et al., 2017). Often these changes display threshold-like behavior with ecosystem processes including wind erosion responding nonlinearly to changes in plant communities and reinforcing trajectories of degradation between alternative ecological states (e.g., grassland to eroded shrubland; Christensen et al., 2023). In susceptible landscapes, the loss of vegetation cover and structural simplification can influence wind erosion and sand and dust storms (SDS) that have far-reaching consequences for Earth systems and society (Shao et al., 2011; Webb & Pierre, 2018). Thus, understanding aeolian sediment transport responses to plant community change is critical for understanding and managing the most pernicious consequences of land degradation.

Funding acquisition: Nicholas P. Webb, Brandon T. Bestelmeyer
Investigation: Nicholas P. Webb, Brandi Wheeler, Brandon L. Edwards, Dawn Browning, Saroj Dhital, Kristina E. Young, Brandon T. Bestelmeyer
Methodology: Nicholas P. Webb, Brandi Wheeler, Brandon L. Edwards, Jeremy W. Schallner, Justin W. Van Zee, Ericha M. Courtright, Sarah E. McCord
Project administration: Nicholas P. Webb, Dawn Browning, Brandon T. Bestelmeyer
Software: Jeremy W. Schallner, Sarah E. McCord
Visualization: Brandi Wheeler
Writing – original draft: Nicholas P. Webb
Writing – review & editing: Brandi Wheeler, Brandon L. Edwards, Jeremy W. Schallner, Neeshia Macanowicz, Justin W. Van Zee, Ericha M. Courtright, Brad Cooper, Sarah E. McCord, Dawn Browning, Saroj Dhital, Kristina E. Young, Brandon T. Bestelmeyer

Several studies have described potential wind erosion responses to ecosystem change at regional and global scales. Simulated climate change impacts on global dust emissions have found widely varying dust emission responses (−63% to +24%) from different terrestrial biosphere models used to describe vegetation change (e.g., Mahowald & Luo, 2003; Tegen et al., 2004; Woodward et al., 2005). Such studies have been constrained by large uncertainties in representing the effects of vegetation and its change specifically in drag partitioning schemes that represent the attenuating effects of vegetation on wind erosivity (Webb et al., 2014a). Consequently, studies seeking to describe drivers of change in observed dust event frequencies, dust concentrations, and dust optical depth have tended to focus on relationships with meteorological drivers (e.g., Achakulwisut et al., 2017; Pu & Ginoux, 2018) and land use change (e.g., Lambert et al., 2020). The effects of regional vegetation change on spatiotemporal patterns of sediment transport have not been quantified with sufficient detail to evaluate implications for dryland management.

Landscape-scale modeling and field studies have more closely examined aeolian process interactions with vegetation disturbances and change. A focus of preceding work has been to establish the magnitude of increases/decreases in aeolian sediment transport rates in response to land cover change and stressors that drive ecosystem degradation and restoration (e.g., Aubault et al., 2015; Burger et al., 2023; Pierre et al., 2021; Treminio et al., 2024; Webb et al., 2014b). For example, experimental approaches have elucidated aeolian process responses to gradients of disturbance, such as grass removal treatments, fire, livestock grazing, and their effects on plant communities (e.g., Dukes et al., 2018; Li et al., 2009; Munkhtsetseg et al., 2017; Sankey et al., 2012; Sasaki et al., 2018). Such work has provided a basis for understanding how aeolian processes respond to ecological state changes (e.g., associated with shrub encroachment), although the literature explicitly addressing the interactions with aeolian processes remains sparse (e.g., Galloza et al., 2018; Miller et al., 2011; Payne et al., 2023; Webb et al., 2020, 2024).

The Chihuahuan Desert is a major North American dust source region that is undergoing extensive ecosystem change (Huenneke et al., 2002). Over the last century, perennial grasslands on sandy soils have been replaced by honey mesquite (*Prosopis glandulosa* Torr.) and creosote bush (*Larrea tridentata* DC) shrubs with grass loss and shrub dominance leading to changes in vegetation height, increased bare ground, and larger spaces between plant canopies (Okin et al., 2006). Drivers of grass loss and ecological state transitions include a combination of drought, climate change, and grazing pressure from native and non-native herbivores (Figure 1; Bestelmeyer et al., 2018). The plant community changes influence patterns of wind shear velocity (King et al., 2006; Ziegler et al., 2023) and affect sediment transport rates and dust emission. Aeolian sediment transport can be both an endogenous and exogenous driver of ecological state change in the system (Payne et al., 2023). For example, grass removal from shrub-invaded grasslands can cause nonlinear increases in horizontal sediment mass flux (Q; g m^{-1} d^{-1}) (Li et al., 2009). In the Jornada Basin, Q at a mesquite shrubland site can be two to three orders of magnitude larger than for other plant communities across a range of soil types (Bergametti & Gillette, 2010; Floyd & Gill, 2011). These findings, and recent modeling by Webb et al. (2024), suggest that changes in plant community composition, cover, and structure, which occur when degradation and restoration thresholds are crossed between ecological states, could have important effects on aeolian sediment transport rates.

Here, our objectives are to: (a) describe changes in vegetation cover and structure associated with ecological state changes at sites on soils that are susceptible to wind erosion; (b) quantify the magnitude and direction of aeolian sediment transport responses to ecological state changes; and (c) identify critical thresholds for increasing and decreasing sediment transport rates and their association with ecological states and transitions. We address these objectives using field measurements of vegetation, meteorological parameters, and aeolian horizontal sediment mass flux across five ecological states of the Chihuahuan Desert that are representative of degradation and restoration pathways typical of drylands globally. We predict that crossing a sequence of degradation thresholds will lead to nonlinear increases in aeolian sediment transport rates consistent with feedback mechanisms assumed to reinforce shrub dominance. We also predict that a state in which natural vegetation recovery has occurred will recover sediment fluxes to rates characteristic of the historical grassland state.

2. Study Area

Our research focus is on the interactions between aeolian sediment transport and ecological state transitions on sandy basin floor landforms that are common in south-central New Mexico, USA (Figure 2). The study area is in a hot desert region with mean annual temperatures ranging from 12°C to greater than 20°C and mean annual

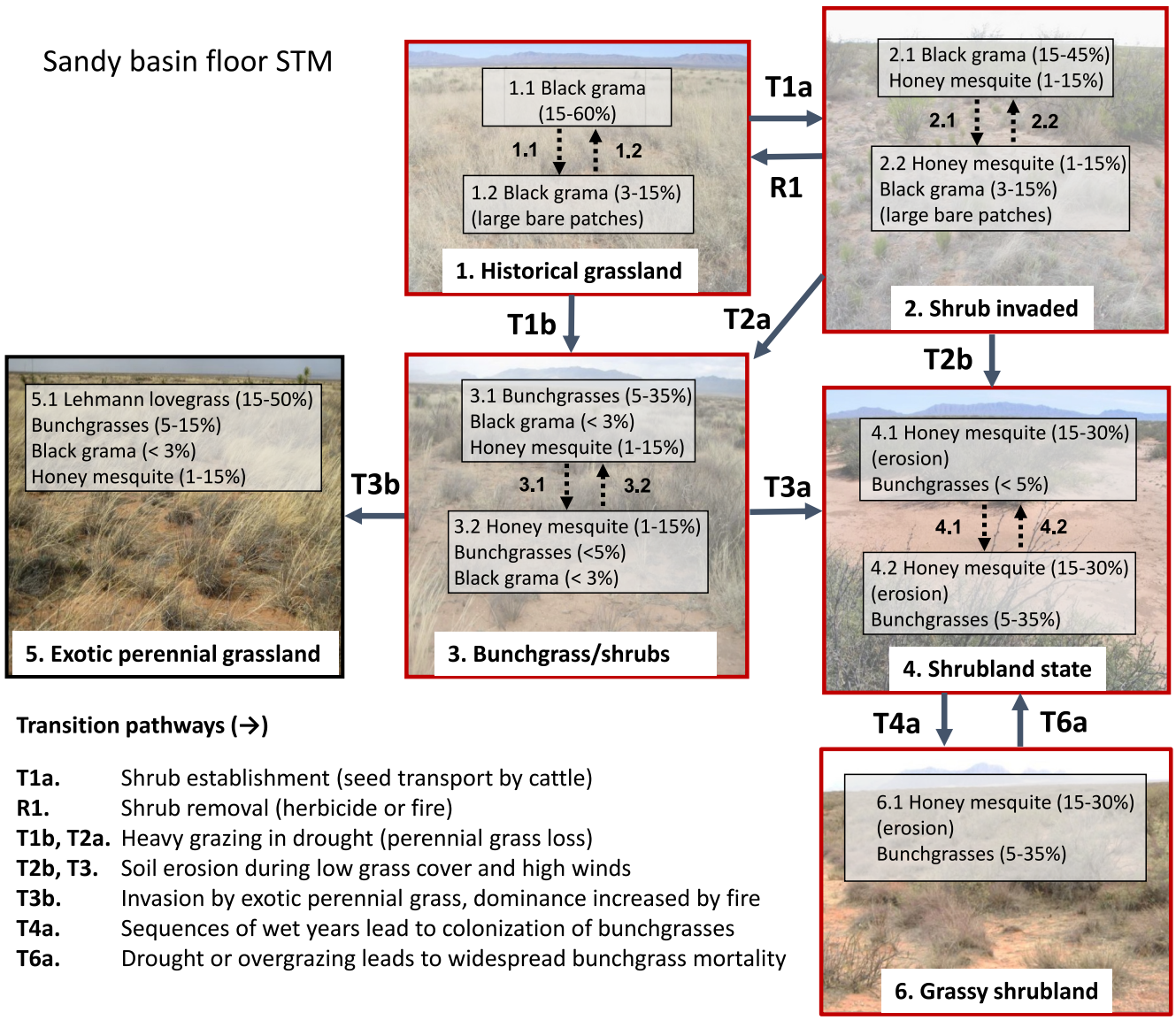

Figure 1. State-and-transition model (STM) for the sandy basin floor landform in the northern Chihuahuan Desert. Focal ecological states are highlighted in red with DuRP study sites in the historical grassland (state 1; HGR), shrubland (state 4; SHR), and grassy shrubland (state 6; GSH). The NWERN site classified to shrub invaded (state 2; SHI), transitioning in spring 2020 to bunchgrass/shrub (state BSH).

precipitation of 200–381 mm with most falling in summer (June to September) (Wainwright, 2006). Wind speeds have strong seasonality with highest wind speeds occurring in spring from a southwesterly to west-southwesterly direction (Bergametti & Gillette, 2010). Predominant soils are moderately deep to deep (0.5–1.5 m) and well drained with fine sandy loam, sandy loam, and loamy fine sand surface textures (Monger, 2006). These soils are intermingled with soils that are shallow (<0.5 m) and well drained with sandy loam, loamy sand to gravelly fine sandy loam texture (Monger, 2006).

The ecological dynamics of sandy basin floor landforms follow a pattern of shrub encroachment, grass loss, and increasing bare ground—summarized in the state-and-transition model (STM) in Figure 1. Historical plant communities (state 1) are dominated by perennial black grama grass (*Bouteloua eriopoda* Torr.) with presence of other perennial grasses such as dropseeds (*Sporobolus spp.*). Prolonged drought and improperly managed grazing lead to the reduction (state 2), fragmentation, or complete loss of black grama and establishment and expansion of deciduous honey mesquite (hereon mesquite). Locations in a mixed bunchgrass/shrub ecological state (state 3) may be susceptible to invasion by the perennial Lehmann lovegrass (*Eragrostis lehmanniana* Nees) leading to

establishment of an invaded grassland state (state 5). Continued improper grazing of remnant grasses (state 3) leads to loss of perennial grasses in shrub interspaces, accelerated aeolian sediment transport and water erosion, and formation of mesquite nebkha dunelands (state 4). Following multiple years of above-average rainfall, perennial bunchgrasses may establish in mesquite shrublands and form a novel grassy shrubland state (state 6), which indicates an event-driven, natural recovery of herbaceous cover but not including the historically dominant black grama (Bestelmeyer et al., 2018).

2.1. Field Monitoring Plots

We used standard vegetation monitoring data collected on the United States Department of Agriculture's (USDA) Jornada Experimental Range (JER) and on the US Department of Interior's Bureau of Land Management (BLM) lands. Jornada Experimental Range data were collected from two long-term studies (Figure S1 in Supporting Information S1). The JER Duneland Restoration Project (DuRP) was established in May 2018 across three locations representing different ecological states: historical grassland with scattered mesquite (HGR; tending to STM state 2.1 based on mesquite presence; located 32.5834°N, 106.8285°W); degraded mesquite shrubland characterized by nebkha dunes (SHR; STM state 4; located 32.6415°N, 106.7662°W); and grassy shrubland (GSH; STM state 6; located 32.6442°N, 106.8364°W). Within each site, a 100 × 100 m plot was established in May 2018 to monitor vegetation cover, composition, and structure, and aeolian sediment transport rates (see Section 3.1).

To include measurements from a site actively undergoing a transition from shrub invaded (SHI; state 2) to bunchgrass/shrub (BSH; state 3), we used data collected at the JER National Wind Erosion Research Network (NWERN) site located 32.6269°N, 106.7387°W (Webb et al., 2016). At the time of establishment (June 2014), the site was in the shrub invaded ecological state (SHI; state 2.2) then in spring 2020 transitioned to bunchgrass/shrubs (BSH; states 3.1 and 3.2). The site was established as a 100 × 100 m plot at which meteorological conditions, vegetation cover, composition, and structure, and aeolian sediment transport rates were monitored. Management across the four JER plots varied with cattle excluded from the pasture in which the HGR plot was located since 2008, the SHR and GSH plots intermittently grazed by cattle, and the SHI plot grazed by cattle until 2022 after which the plot was fenced to exclude cattle grazing. All plots were grazed by native herbivores and introduced *Oryx gazella*.

As it was impractical to replicate the study sites due to the intensity of our sampling (see Section 3.1), we used compatible data sets to understand the representativeness of our sites and provide regional context for the analysis. Specifically, we used standardized data collected at 142 monitoring plots by the BLM Assessment, Inventory and Monitoring (AIM) program (Kachergis et al., 2022; Yu et al., 2020). The monitoring program was established in 2011 and collects data annually to inform management of public lands administered by the BLM.

3. Methods

3.1. Data Collection

At each of the HGR, SHI, SHR, GSH, and AIM monitoring plots, vegetation data were collected using the standard methods of Herrick et al. (2018), including line-point intercept (LPI), all-plant canopy gap intercept, and vegetation height. At the HGR, SHR, and GSH plots, the standard methods were implemented on three 30 m transects starting 5 m from the plot centers, and at the SHI plot on three 100 m transects crossing at the plot centers, oriented from 0 to 180°, 60–240°, and 120–300°. The LPI method was implemented with sampling frequency of 0.25 m at the HGR, SHR, GSH, and SHI plots. Vegetation height of the tallest species was recorded every 2.0 m at HGR, SHR, GSH, and SHI plots. At the AIM plots, one of two plot-level sample designs was used. At 129 AIM plots, the standard methods were implemented on three 50 m transects, starting 5 m from the plot center and oriented 120° apart with the first transect set at 0° or a randomized azimuth. The LPI method was implemented with sampling frequency of 0.5 m and vegetation height of the tallest woody and tallest herbaceous species, respectively, were recorded every 5 m. At 13 AIM plots, the standard methods were implemented on two 45.72 m (150 ft) transects oriented 45–125° and 135–315° and crossing at the center. The LPI method was implemented with sampling frequency of 0.91 m (3 ft) and vegetation height of the tallest woody and tallest herbaceous species, respectively, every 3.05 m (10 ft). Transects were sampled at the HGR, SHR, and GSH plots in May 2018 and August 2020, 2021, and 2023, and September 2022. Transects were sampled three to four times per year (generally, March, June, September, and December) at the SHI plot to capture seasonal differences in vegetation cover and structure. The AIM plots were sampled once each (between September to November) from 2011 to 2023.

At the SHI plot, a central meteorological tower instrumented with RM Young 3101 cup anemometers at 0.5, 1.0, 1.5, 2.5, and 5.0 m and an RM Young 3002 cup anemometer with wind vane at 10 m above ground level (AGL) to measure the vertical wind speed profile. Naturally aspirated shield temperature sensors (model 107-L) mounted at 2.0 and 10.0 m and Campbell Scientific EE181 model air temperature/relative humidity probe mounted at 4.0 m AGL measured the air temperature profile. A Texas Instruments tipping bucket rain gauge (TE105) recorded precipitation at 1.5 m AGL adjacent to the tower. Meteorological data were sampled at 1 Hz and recorded at 1 min resolution on a Campbell Scientific Inc. CR1000 data logger.

At the HGR, SHR, GSH, and SHI plots, the horizontal sediment mass flux was monitored using stratified random sample designs with nine (HGR, SHR, and GSH) and 27 (SHI) Modified Wilson and Cooke (MWAC) sediment sampler masts (Webb et al., 2019). The MWAC masts were equipped with samplers with center of inlets maintained at 0.10, 0.25, 0.50, and 0.85 m heights AGL (Webb et al., 2015). Stratification was provided by a regular 3 × 3 square grid (each 33.3 m^2) and one (HGR, SHR, and GSH) or three (SHI) MWAC masts were located randomly within each grid cell. The HGR, SHR, and GSH MWAC samplers had inlet areas of 4.71×10^{-5} m^2 from 14 May 2018 until 16 November 2020 at which time they were changed to 2.34×10^{-4} m^2 to be consistent with the SHI MWAC samplers. Sediment trapped in the MWAC samplers was collected approximately every 28 days from May 2018 to July 2023 at the HGR, SHR, and GSH plots, and data were collected at the same frequency from January 2015 to March 2024 at the SHI plot. Sediment was extracted from the samplers following either dry (HGR, SHR, and GSH) or wet (SHI) extraction protocols and weighed to determine sediment masses following Webb et al. (2015).

3.2. Data Analysis

Plot-level vegetation data were harmonized then aggregated using the *terradactyl* R package (McCord et al., 2022) and managed in the Landscape Data Commons (McCord et al., 2023). Using *terradactyl*, ground cover indicators were calculated from the monitoring data, including total foliar cover (%), plant species cover (%), plant functional group cover (%), bare soil (%), occurrence of canopy gaps in size classes of 25–50, 51–100, >100, and >200 cm (%), and the average maximum (woody or herbaceous) vegetation height (cm). Indicators for each sampling event were tabulated for comparison and, for SHI, plotted to examine seasonal and monotonic trends.

Wind speed data from the SHI plot were summarized in wind roses to visualize the directional distribution of wind speeds among seasons. Using the Prandtl-von Kármán logarithmic velocity profile law following Webb et al. (2021), running average (15 min) wind speed collected at the SHI plot from 2015 to 2024 were used to calculate the aerodynamic roughness length (z_0) and wind shear velocity (u_*). We also calculated the normalized shear velocity (u_*/U_{10}) used in drag partitioning studies with smaller/larger values indicating smaller/larger aerodynamic roughness of the vegetation canopy and larger/smaller (i.e., the inverse) wind shear velocity at the soil surface (Ziegler et al., 2023). Precipitation data from the SHI plot were summarized to monthly totals (mm) from 2015 to 2024 to provide context for the vegetation growing conditions.

We calculated vertically integrated horizontal sediment mass fluxes (Q) from the sediment masses collected at each MWAC mast normalized by the MWAC inlet areas using nonlinear least squares regression to fit exponential functions to the data. Following Webb et al. (2019), we then fitted two-parameter or three-parameter functions to the mass flux profiles depending on whether sediment masses of detectable weight (>0.0001 g) were available at three or four heights, respectively (76% of total samples). We then integrated from 0 to 1.0 m height and divided by the sampling periods to obtain:

$$Q = \int_0^1 q(z)\, dz, \tag{1}$$

where $q(z)$ is the sediment mass collected per unit inlet area (m^{-2}) per sampling period (day) at heights z (m), and Q is expressed with units of g m^{-1} d^{-1}. Horvitz-Thomson estimators of the mass flux mean, spatial variance ($\widehat{\overline{V}}_s$), and their temporal variances ($\widehat{\overline{V}}_t$) in each season were calculated following Webb et al. (2019).

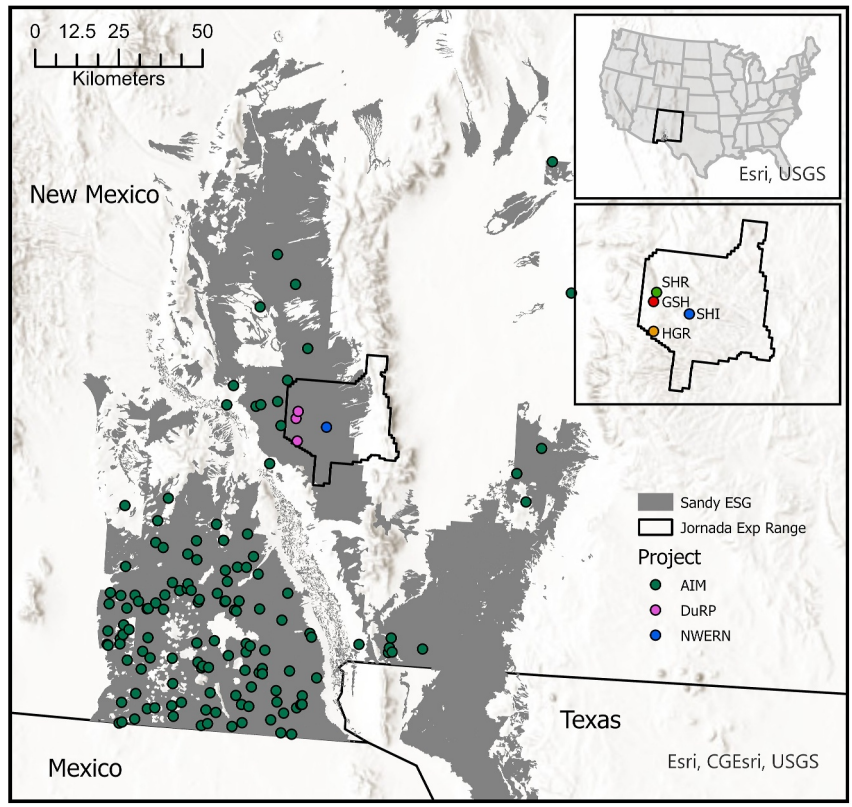

Figure 2. Study area map showing the spatial extent of the Sandy ecological site group (ESG) in south-central New Mexico, USA (upper inset map), location of DuRP, NWERN, and AIM monitoring plots, and specific locations of the DuRP black grama (HGR), shrubland (SHR) and grassy shrubland (GSH) plots, and shrub invaded (SHI) NWERN site within the Jornada Experimental Range (lower inset map).

We compared seasonal total Q at the HGR, SHR, GSH, and SHI plots (2018–2023) using nonparametric Kruskal-Wallis tests and pairwise Wilcoxon rank sum tests with Bonferroni adjustment to evaluate whether the magnitude of Q differed significantly between ecological states. For the SHI plot, daily average wind speed at 10 m AGL (U_{10}), z_0, and u_*/U_{10}, and monthly Q (2015–2024) were plotted and seasonal nonparametric Mann-Kendall's tests for trend (Gilbert, 1987; Hirsch et al., 1982) were run on each variable to test for monotonic trends in the aerodynamic properties and sediment mass fluxes before and after the site transitioned from the shrub invaded to bunchgrass/shrub state (Figure 2). Analyses were conducted in R (version 4.3.1) using the *stats* and *EnvStats* packages (Millard, 2013).

4. Results

4.1. Plot Vegetation Characteristics Across Ecological States

Vegetation monitoring data show how the composition, cover, and structure of vegetation differed among ecological states at the HGR, SHR, GSH, and SHI plots (Table 1). At the HGR plot, total foliar cover ranged from 34.7% to 79.7% with perennial forb and grass cover 23.1%–40% and mesquite shrub cover 3.9%–7.2%. Bare (unvegetated) soil was 17.5%–39.4% with all-plant canopy gaps tending to <100 cm and, from 2018 to 2022, less than 20% of the plot area having gaps >200 cm. A decline in total foliar cover, associated with an increase in mesquite shrub cover and larger decrease in perennial forb and grass cover, is characteristic of the transition—from historical grassland to the shrub invaded state—reflected in the indicators for the SHI plot in 2015. The increase in bare ground at SHI is reflected in our measured relatively large (>100 cm) and very large (>200 cm) all-plant canopy gaps, shorter height of grasses, and small increase in the height of mesquite shrubs relative to the HGR plot. Indicators at the SHR plot reflect transition to the shrubland state, with bare soil at the plot

Table 1
Summary of Vegetation Cover and Structure Indicators at the Monitoring Plots

		Percent cover (%)									Height (cm)	
Plot ID	Date (yyyy-mm-dd)	Bare soil	Total foliar	Peren. forb grass	Shrub	Peren. grass	Canopy gap 25–50 cm	Canopy gap 51–100 cm	Canopy Gap 101–200 cm	Canopy gap >200 cm	Mean grass	Mean woody
HGR	2018-05-10	28.6	46.9	40.0	3.9	38.9	13.0	20.4	10.9	13.7	43.0	59.0
	2020-08-19	33.6	43.6	30.6	6.4	28.3	9.4	28.2	8.4	18.9	41.5	69.2
	2021-08-25	15.8	79.7	35.6	7.2	33.3	15.3	3.9	3.8	0	47.3	74.3
	2022-09-19	17.5	54.7	33.3	6.4	32.8	16.8	14.1	20.8	3.4	38.0	65.7
	2023-08-31	39.4	34.7	23.1	6.9	22.8	4.5	23.2	13.3	30.7	35.9	5.71
SHI	2018-06-11	68.7	23.8	12.9	13.4	11.2	3.6	10.6	20.4	44.8	20.6	74.6
	2020-09-15	68.5	25.9	8.1	16.9	5.82	4.1	12.7	19.3	38.9	11.7	68.1
	2021-09-22	68.3	24.8	6.4	16.3	5.48	3.1	11.3	20.3	42.9	14.2	67.3
	2022-09-23	71.5	22.2	6.2	15.5	4.89	3.1	8.3	16.3	52.1	14.5	68.2
	2023-09-14	64.2	17.1	3.5	13.1	3.3	2.4	6.4	11.2	64.6	12.7	59.3
SHR	2018-06-21	63.6	22.8	0.0	19.7	0.0	2.2	2.6	5.6	68.9	-	63.4
	2020-08-20	57.2	25.0	0.0	21.4	0.0	2.2	1.7	8.3	62.7	1.0	65.9
	2021-08-25	59.7	21.4	0.0	18.1	0.0	3.0	3.5	8.5	60.0	9.0	66.1
	2022-09-19	65.6	19.4	0.0	17.2	0.0	2.6	3.4	5.7	65.0	-	59.1
	2023-08-31	65.6	21.9	0.3	19.7	0.3	3.8	2.8	7.5	63.7	-	66.8
GSH	2018-06-21	40.0	39.4	32.2	18.9	31.9	0.6	7.2	11.4	46.3	26.2	72.9
	2020-08-20	43.3	44.2	29.7	21.1	29.7	2.2	5.3	8.4	44.5	49.2	59.6
	2021-08-25	41.9	46.4	33.1	20.0	33.1	1.8	12.3	14.3	32.4	34.7	63.5
	2022-09-19	35.3	49.2	28.1	18.1	28.1	8.9	11.9	18.0	14.4	37.1	66.9
	2023-08-31	45.0	34.7	21.4	16.1	21.4	3.9	7.0	12.8	48.7	21.6	61.7

Note. Data for the SHI plot are shown only for dates approximately consistent with the HGR, SHR, and GSH plot sampling events. Complete timeseries (2015–2024) of the indicators are shown for the SHI plot in Figure 5.

57.2%–65.6%, near complete loss of perennial forbs and grasses and remaining ground cover (19.4%–25.0%) comprised predominantly of mesquite shrub cover (17.2%–21.4%). The structural indicators for the SHR plot also show differences with shrub height consistent with the HGR and SHI plots but occurrence of >200 cm canopy gaps increasing to 60.0%–68.9%. Mesquite shrub cover at the GSH plot was similar to that of the SHR plot while percent bare soil (35.3%–45.0%) was lower and total foliar cover was higher with perennial forb and grass cover 21.4%–32.2%. Although shrub heights were consistent with HGR and SHR, grasses at the GSH plot are an important structural element (21.6–49.2 cm heights) and the occurrence of >100 cm (8.4%–18.0%) and >200 cm (14.4%–48.7%) canopy gaps were lower than for the SHR plot—consistent with the shrub interspaces being occupied by perennial forbs and grasses.

To understand the representativeness of the study plots in a regional context, we evaluated the cover of perennial forbs and grasses and shrubs relative to BLM AIM plots sampled across the northern Chihuahuan Desert (Figure 3). Our data show that the HGR, SHI, and SHR plots fall within the expected ranges of the plant functional groups and species cover in the region. Plots with low shrub cover can have high perennial forb and grass cover (e.g., HGR), whereas plots with high shrub cover tend to have low perennial forb and grass cover (e.g., SHR). The SHI plot measurements spanned the intermediate space, reflective of the shrub invaded and bunchgrass/shrub states having a broad range in cover of different plant functional groups. Measurements at the GSH plot (state 6) suggest novelty of the plot location or ecological state—consistent with few sites in the region having crossed the restorative threshold that enabled perennial forb and grass establishment in a mesquite shrubland.

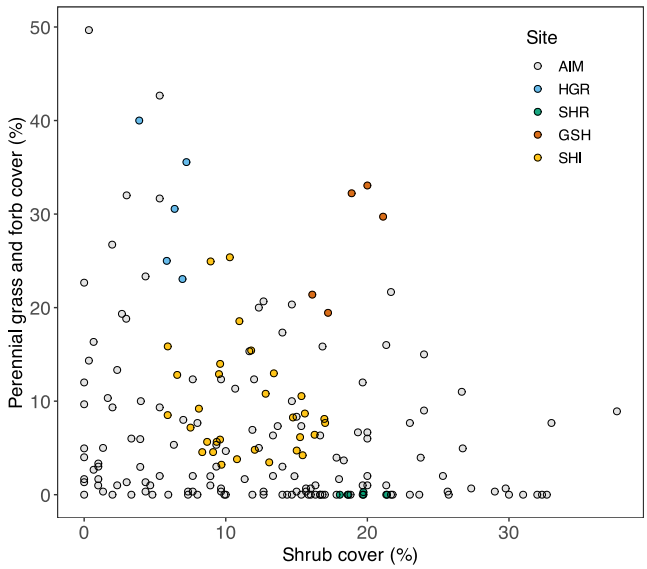

Figure 3. Relationship between perennial grass and forb cover and shrub cover for the historical grassland (HGR), shrubland (SHR), and grassy shrubland (GSH) plots (repeat sampled 2018 to 2023), and shrub invaded (SHI) plot (repeat sampled 2015 to 2023) on the Jornada Experimental Range relative to AIM plots sampled regionally on BLM lands from 2011 to 2022.

4.2. Magnitude Shifts in Aeolian Sediment Transport

There were statistically significant, order of magnitude increases in aeolian horizontal sediment mass flux (Q) from the HGR, to SHI, to SHR plots (Figure 4). Although Q was typically ~1–10 g m^{-1} d^{-1} at the HGR plot, the sediment transport rate increased to ~10–100 g m^{-1} d^{-1} at the SHI plot and in 54% of sampled seasons ~100–10,000 g m^{-1} d^{-1} at the SHR plot. We also found statistically significant, order of magnitude differences between Q for the GSH plot (~1–10 g m^{-1} d^{-1}) and SHR and SHI plots. Increases in Q across the ecological state changes follow the pattern of perennial forb and grass loss and increasing shrub cover, indicating ecological state changes across degradation thresholds can result in significant increases in sediment transport. Conversely, crossing a restorative threshold effectively reduced Q at the GSH plot to rates consistent with the HGR plot.

We also observed large seasonal variability in Q and its differences between plots, consistent with strong seasonal variability in wind speeds (Figure S2 in Supporting Information S1). Significant differences in Q between plots in the different ecological states were most pronounced in spring (March, April, and May). Spring was also the only season with a significant difference in Q between the HGR and GSH plots in 2022. In all other seasons and years, the magnitude of Q in the HGR and GSH plots was statistically the same. The difference in Q between HGR and SHI plots also showed some variability among seasons depending on year. Differences in Q between the plots representing different ecological states were smallest, or absent, during summer (June, July, and August) in the year 2020. Sediment mass fluxes were typically largest in spring and winter (December, January, and February) and smallest in summer and fall (September, October, and November). The spatial and temporal variability of Q increased progressively across the degradation gradient with the SHR plot having the largest mean Q and large spatial and temporal variances in all seasons (Table 2). The spatial variability of Q was generally larger for the SHI and SHR plots than for the HGR and GSH plots, but that pattern was not necessarily consistent across the sampled years. Extreme variance in Q during spring and winter at the SHR plot suggest possible under-sampling ($n = 9$ MWAC masts) of the large variability in sediment transport at the plot. Spatial and temporal variability of Q at the GSH plot were consistent with the HGR plot in spring and summer but were larger in fall and winter.

4.3. Sediment Transport Through a State Transition

The SHI plot underwent transition from shrub invaded to bunchgrass/shrub in spring 2020 following a trajectory toward the shrubland state. Time series vegetation cover and structure indicators show an increase in percent bare soil from 2015 to 2024, with decline in total foliar cover (from ~30% to 15%) associated with ~20% decrease in perennial forb and grass cover and concomitant increase in mesquite shrub cover (Figure 5). Seasonal variability of the total foliar cover was dominated by changing shrub cover associated with phenological stages (dormancy, green-up, and leaf-on) of the deciduous mesquite. Seasonal variability was also evident in all-plant canopy gap sizes, with the change from 20% to 70% occurrence of canopy gaps >200 cm having seasonal variability of ~20%, attributable to summer precipitation, and mesquite canopy change and reductions in forb and grass cover during winter. Canopy gap sizes <200 cm showed smaller seasonal variability and consistent reductions from 2015 to 2024. Heights of forbs and shrubs were consistent over the study period with a decline in grass height associated with progressive loss of grasses from the plot. The small decline in shrub height after 2022 may reflect increased sediment trapping, which effectively raises the ground level from which vegetation height measurements were made.

We found no trend in U_{10} and statistically significant ($p < 0.05$) but weak negative trends in U_{10} at the SHI plot in all seasons of 2015–2019, and significant positive trends in U_{10} in all seasons after 2020 when the plot transitioned to the BSH state (Figure 6; Table S1 in Supporting Information S1). We found consistent trends in z_0 (Figure 7) and u_*/U_{10} (Figure 8) for the same periods, with both z_0 and u_*/U_{10} having positive trends in summer in the SHI state and in fall and winter for the BSH state, and z_0 and u_*/U_{10} having negative trends in spring in the

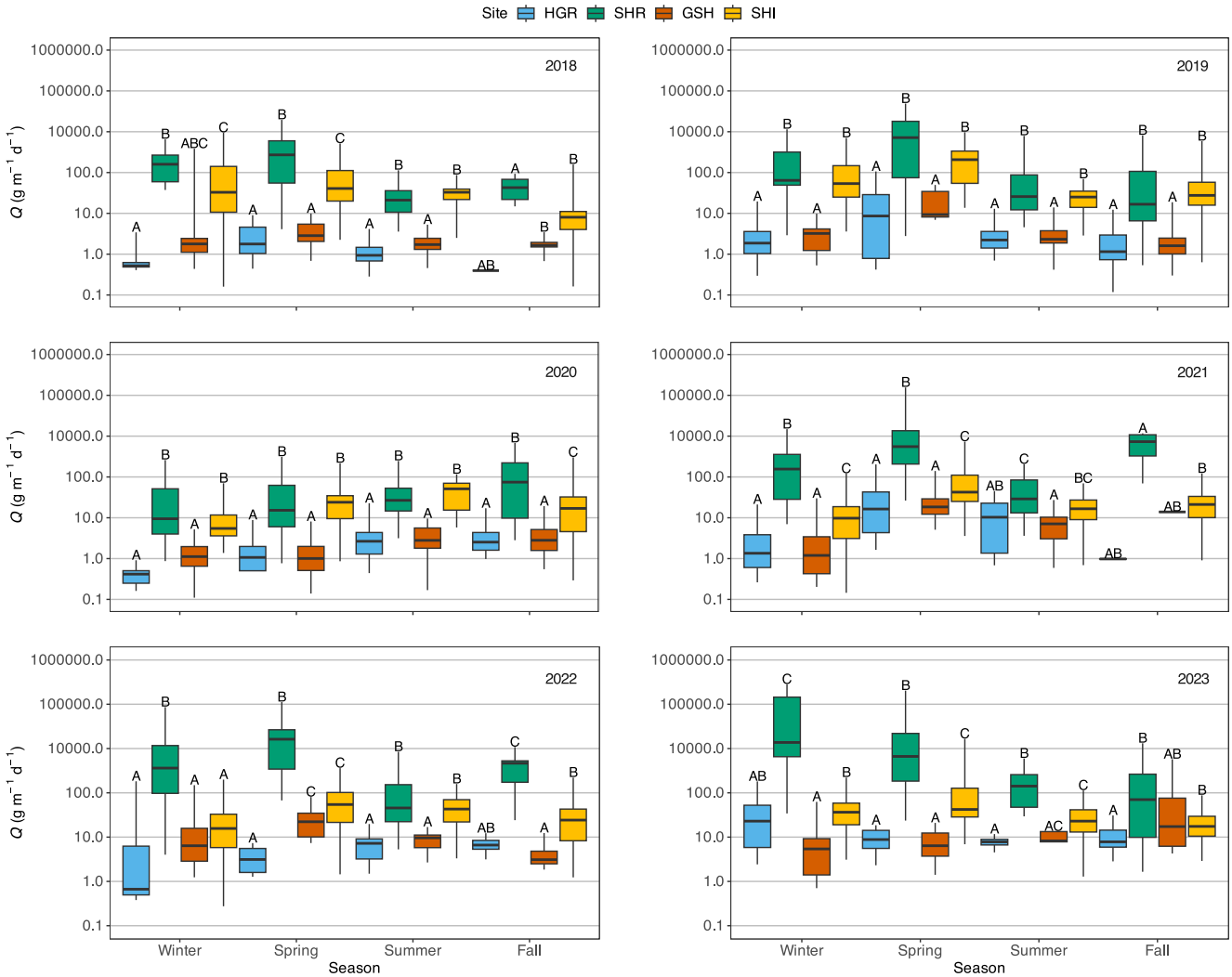

Figure 4. Box-and-whisker plots of measured monthly horizontal sediment mass flux Q (g m^{-1} d^{-1}) within each season at the historic grassland (HGR - blue), shrubland (SHR - green), grassy shrubland (GSH - red), and shrub invaded (SHI - orange) plots from spring 2018 through winter 2023. Boxes show median and interquartile ranges of Q, whereas whiskers show ranges of remaining data. Letters (A, B, and C) indicate statistically significant differences in Q between plots within a season, identified using pairwise Wilcoxon rank sum tests with Bonferroni adjustment.

BSH state. With average shrub height over the study period ~69.7 cm, it is possible that U_{10} is not high enough in the atmospheric boundary layer to be fully independent of the surface roughness. However, the negative trend in z_0 and u_*/U_{10} in spring are consistent with the measured changes in vegetation cover and large increase in canopy gaps >200 cm. Decreasing z_0 and u_*/U_{10} indicate from 2020 to 2024, there was a reduced aerodynamic effect of vegetation following the state transition. Conversely, we observed weak positive trends of the aerodynamic properties during summer and fall when the mesquite shrubs had leaves. Following the patterns of vegetation cover, structure, and wind speed, z_0 and u_*/U_{10} exhibited seasonal and interannual variability with the strength of the seasonal variability especially large in 2024 and influencing winter and fall trends.

Time series of Q showed large inter and intra-annual variability at the SHI plot (Figure 9). Transition from the shrub invaded state to bunchgrass/shrub state appeared to have no effect on the magnitude or trend of Q during summer and fall. The data show a nonsignificant positive trends in Q during winter and spring, following large variability in Q from 2015 to 2019, before increasing each year to 2024. Days with daily average wind speeds >10 m s^{-1} in each year prior to the state transition sometimes increased Q toward 1,000 g m^{-1} d^{-1}—for example in 2017 and 2019 and in 2023 and 2024 after the plot transitioned to the bunchgrass/shrub state. Comparison with Figure 4 shows that, for almost half the sampling events, Q at the SHI plot was within ±1 order of magnitude of

Table 2
Seasonal Mean, Spatial Variances ($\widehat{V}_s$), and Temporal Variances ($\widehat{V}_t$) of Horizontal Sediment Mass Fluxes Q (g m^{-1} d^{-1}) for the Study Plots Calculated From Stratified Random Samples of Q

Plot ID	Season	Mean Q (g m^{-1} d^{-1})	Mean spatial variance $\widehat{V}_s$	Mean temporal variance $\widehat{V}_t$
HGR	Spring	10.84	476.26	686.20
	Summer	6.55	82.38	65.69
	Fall	3.53	9.83	21.41
	Winter	3.66	272.23	583.3
SHI	Spring	124.18	19,634.31	36,197.69
	Summer	34.38	552.36	706.47
	Fall	22.15	987.23	3,287.03
	Winter	65.98	9,827.05	13,142.63
SHR	Spring	1,304.39	4,798,448.76	5,395,818.02
	Summer	99.5	17,274.77	17,413.92
	Fall	109.92	31,680.88	60,178.42
	Winter	1,443.37	4,947,629.28	15,265,991.74
GSH	Spring	10.25	228.8	238.35
	Summer	5.52	16.87	21.95
	Fall	12.15	2,031.17	3,349.98
	Winter	21.61	5,258.76	4,200.43

Note. Data were collected from spring 2018 to fall 2023 (HGR, SHR, GSH) and summer 2015 to spring 2024 (SHI).

the SHR plot (~100–10,000 g m^{-1} d^{-1}) while Q at the HGR and GSH plots were similar and consistent with less windy sampling periods since 2018.

4.4. Critical Ecological and Cover Thresholds for Aeolian Sediment Transport

The relationship between perennial grass cover, ecological state, and Q revealed critical ecological thresholds above/below which we observed order-of-magnitude increases/decreases in aeolian sediment transport (Figure 10). With exception of a few extreme wind events, the first order-of-magnitude increase in Q, from ~1 to 10 g m^{-1} d^{-1} to ~10–100 g m^{-1} d^{-1}, occurred within the shrub invaded ecological state when perennial grass cover dropped below ~20%. The sediment transport rate increased again when perennial grass cover dropped below ~10% around the transition from the shrub invaded state to the bunchgrass/shrub state. The third order-of-magnitude increase in Q, from ~10 to 100 g m^{-1} d^{-1} to 100–10,000 g m^{-1} d^{-1} between the bunchgrass/shrub state and shrubland state, occurred when perennial grass cover dropped below ~5%. The ~20% perennial grass cover threshold for the first magnitude increase in Q was consistent with the multiple orders-of-magnitude decrease in Q from 100 to 10,000 g m^{-1} d^{-1} to ~1–10 g m^{-1} d^{-1} between the shrubland and grassy shrubland states.

5. Discussion

Wind erosion and SDS have far-reaching consequences for Earth systems and society. Understanding the relationship between ecological state change and wind erosion is essential for effective management. Here, we predicted that crossing a sequence of degradation thresholds associated with ecological state changes will lead to nonlinear increases in aeolian sediment transport rates consistent with feedback mechanisms assumed to reinforce shrub dominance in drylands. We also predicted that natural recovery of perennial grasses will lead to recovery of ecosystem process rates (in this case, sediment fluxes) characteristic of the historical grassland state. Our results confirm our hypotheses revealing that order-of-magnitude shifts in aeolian sediment transport rates are associated with plant community changes among ecological states in our study ecosystem. Space-for-time substitution, with simultaneous measurement of different ecological states, enabled us to quantify how state changes can result in step increases in horizontal sediment flux—from ~1 to 10 g m^{-1} d^{-1} in the historical grassland with scattered shrubs, to ~10–100 g m^{-1} d^{-1} following decline in perennial grass cover and increase in shrub cover, to

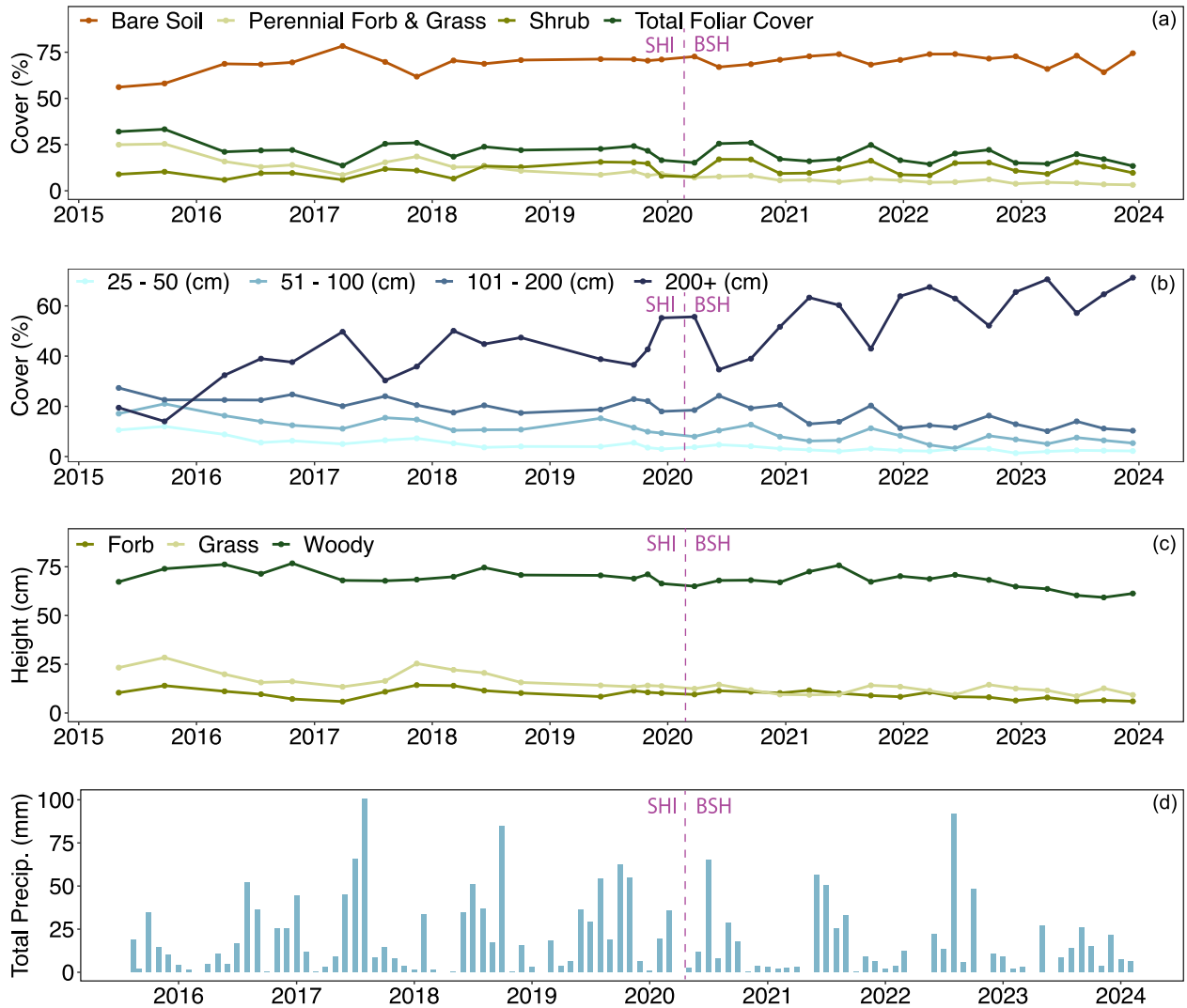

Figure 5. Time series of (a) percent cover of cover types, (b) percent cover of all-plant canopy gap size classes, and (c) mean height of plant functional groups at the SHI plot sampled from spring 2015 to spring 2024. Panel (d) shows time series monthly total precipitation (mm) measured at the center of the plot.

~100–10,000 g m^{-1} d^{-1} in the shrubland state following complete grass loss. These magnitude shifts were associated with critical perennial grass cover thresholds governing sediment fluxes. Following the seasonal pattern of wind speeds, differences were greatest during the spring windy season and smallest during the summer growing season. Our analysis also showed that grass recovery in mesquite shrubland can effectively reduce aeolian sediment transport to rates similar to those in historical grasslands—a potentially multiple order-of-magnitude reduction. These findings have important implications for understanding controls on wind erosion and desertification in drylands, and can guide management while providing insights to effective modes of ecological restoration.

Mechanistically, the observed magnitude shifts in sediment transport across perennial grass cover thresholds are related to vegetation structural changes that occur among ecological states. The first magnitude shift in sediment flux occurred following shrub invasion of historical grassland, when perennial grass cover fell below ~20%. The threshold is consistent with a plant community phase shift (Figure 2) as perennial grass cover declined from 15% to 45% (state 2.1) to 13%–25% (state 2.2). The second magnitude shift occurred when perennial grass cover fell below ~10%, in the bunchgrass/shrub ecological state with plant community phase shift from state 3.1 to state 3.2 (Figure 2). The third magnitude shift occurred when perennial grass cover fell below ~5%, coincident with the state transition from the bunchgrass/shrub state to shrubland. These thresholds are generally consistent with

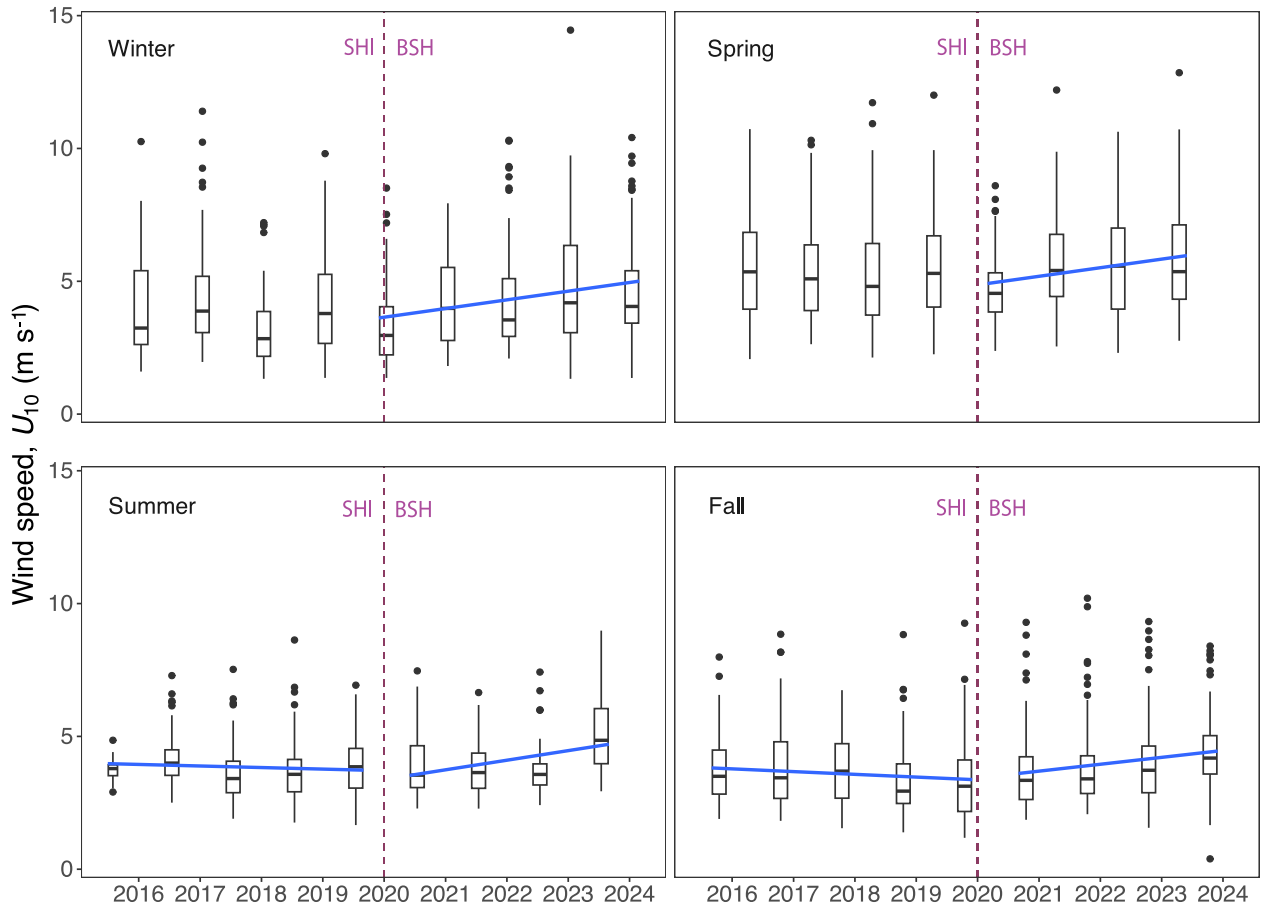

Figure 6. Seasonal wind speed at 10 m AGL, U_{10} (m s^{-1}) from 2015 to 2024 at the SHI site. Blue lines show statistically significant ($P < 0.05$) trends based on Mann-Kendall trend analyses. Vertical dashed lines indicate timing of transition of the site from the shrub invaded (SHI) state to the bunchgrass/shrub (BSH) state.

observations from previous studies in other dryland regions, with Hesse et al. (2017) noting variability in the relationship between aeolian sediment transport and vegetation cover arising from the influence of different vegetation growth habits and forms on drag partitioning. For example, Wiggs et al. (1995) observed a vegetation cover threshold of ~14%, below which sediment transport on linear dunes in the Kalahari Desert increased, whereas Lancaster and Baas (1998) reported a 90% reduction in sand flux between 10% and 15% salt grass cover at Owens Lake, CA. Vegetation cover thresholds are, therefore, likely specific to plant communities that persist in certain soil and landscape settings, with the height and spacing of plants moderating sediment fluxes by controlling drag partitioning and the fetch length over which saltation can establish (Webb, McCord, et al., 2021).

Grass loss across the ecological states led to increased bare soil, which was increasingly distributed in large (>200 cm) gaps between dispersed plant canopies (Table 1). The increase in bare ground and large gaps occurred concurrently with smaller increases in shrub cover. With no large change in shrub height, the net effect was increased exposure of soils to erosive winds. Larger bare spaces between plant canopies mean less aerodynamic sheltering and greater u_{s*} that could entrain and transport sediment (Okin, 2008; Webb et al., 2014a). Aeolian sediment fluxes scale exponentially with u_{s*} such that, as bare ground and all-plant canopy gap sizes increase (with little change in maximum vegetation height), sediment transport rates increase at faster rates (McCord et al., 2023; Wojcikiewicz et al., 2023). Thus, grass loss reduced the aerodynamic roughness, increased soil exposure to the wind, and enabled larger sediment transport rates. With fewer plants to intercept the wind or saltating grains, the saltation flux is more likely to approach saturation as sites transition to the shrubland state (Gillies et al., 2014). This effect was most pronounced in spring when regular sustained high wind speeds (Figure 6) coincided with maximum bare ground and large canopy gaps (Figure 5), increasing the potential for nonlinear changes in sediment transport and differences among states. In summer, variability in sediment fluxes

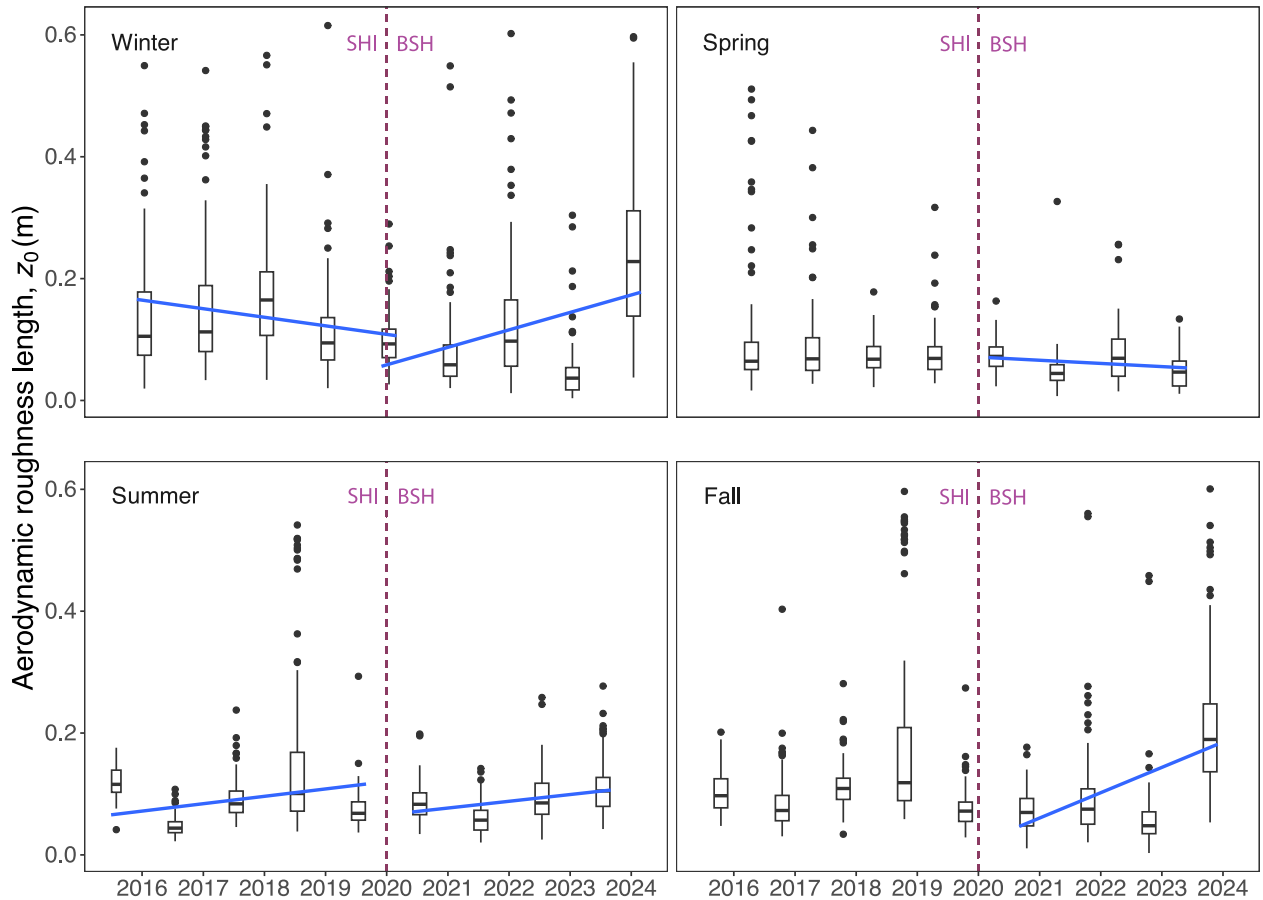

Figure 7. Seasonal aerodynamic roughness length, z_0 (m) from 2015 to 2024 at the SHI site. Blue lines show statistically significant ($P < 0.05$) trends based on Mann-Kendall trend analyses. Vertical dashed lines indicate timing of transition of the site from the shrub invaded (SHI) state to the bunchgrass/shrub (BSH) state.

among ecological states was smaller, as wind speeds were lower and increased ground cover and smaller canopy gaps increased u_*/U_{10} (reducing u_{s*}). These measured responses are consistent with the drag partitioning studies of King et al. (2006) and Ziegler et al. (2023), which showed considerable increase in u_{s*} (i.e., reduction in drag partitioning) between our measured shrub invaded plot and a location in the mesquite shrubland state.

Our measurements support observations that the shifting magnitude of sediment transport across ecological states results in progressive scouring, pedestaling, and loss of perennial grasses, and sediment trapping by shrubs to form nebkha dunes (Gillette et al., 2006). Deflation of soils in canopy gaps has been shown to increase risk of further grass loss through root exposure and abrasion during extreme erosive events (Niu et al., 2023). The increased sediment movement and its biogeochemical impacts are important endogenous feedbacks driving ecological state change and desertification (Li et al., 2009; Okin et al., 2006) and, under extreme erosive events, may act as an exogenous stressor—exposing plant roots and killing perennial grasses—promoting state change (Payne et al., 2023). Building on the findings of Bergametti and Gillette (2010), our results suggest that patterns of aeolian sediment transport likely reflect the important role of spatial heterogeneity in soil-vegetation characteristics. Such a response is consistent with studies showing change in sediment transport rates associated with ecological disturbances in other drylands (e.g., Miller et al., 2011; Sasaki et al., 2018; Webb et al., 2020; Zheng et al., 2021).

5.1. Implications for Wind Erosion Patterns and SDS Management

Our results have broad implications for understanding and managing wind erosion and SDS source areas globally. The ecological dynamics of our study area reflect the dynamics of many dryland ecosystems around the world

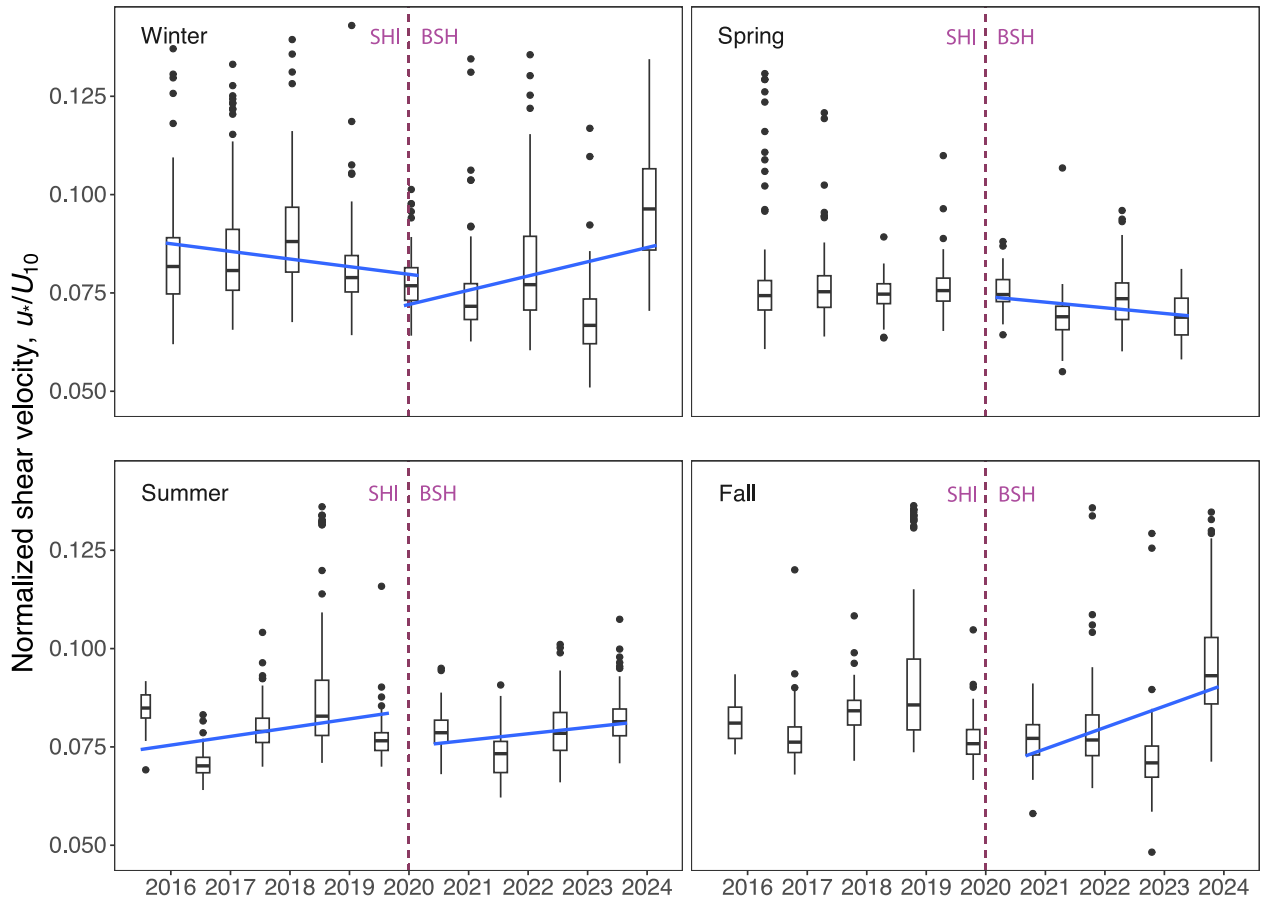

Figure 8. Seasonal normalized wind shear velocity, u_*/U_{10} from 2015 to 2024 at the SHI site. Blue lines show statistically significant ($P < 0.05$) trends based on Mann-Kendall trend analyses. Vertical dashed lines indicate timing of transition of the site from the shrub invaded (SHI) state to the bunchgrass/shrub (BSH) state.

(D'Odorico et al., 2013; Bestelmeyer et al., 2015). Thus, our findings suggest that there is potentially a much greater level of complexity in the controls on wind erosion and SDS than has been recognized in previous regional and global aeolian studies. Although weather and climate undoubtedly influence wind erosion and dust emission rates (Pu & Ginoux, 2018; Robinson & Ardon-Dryer, 2024), our results show that ecological state can have a profound effect on the magnitude and spatiotemporal variability of aeolian sediment transport and could have primacy in determining patterns of wind erosion and dust emissions in vegetated drylands. Elevated aeolian sediment transport rates can accelerate grass loss and associated decline in ecosystem function and services resulting in desertification (UNCCD, 2022). Such changes reduce options available to land managers to mitigate wind erosion, SDS, and undesirable ecological state changes and compromise the efficacy of adaptation to global change pressures such as drought and climate change (Webb et al., 2017).

Specific to our study area, we found sites in the shrub invaded state are at increased risk of wind erosion and should be prioritized for management to avoid perennial grass loss below ~20% cover. If perennial grass cover drops below this threshold, a state change to bunchgrass/shrubs may be difficult to avoid if sediment fluxes increase because site stability is likely to be compromised with scouring/deflation, reduction in soil crust integrity, nutrient and carbon loss from plant interspaces, root exposure, and plant tissue abrasion (Alvarez et al., 2012; Okin et al., 2018). Our results also suggest that the multiple orders-of-magnitude increase in sediment transport associated with the bunchgrass/shrub to shrubland transition depends on only a small change in ground cover—possibly <5% cover of forbs and grasses. Prioritizing maintenance of remaining grass and forb cover in the bunchgrass/shrub state could, therefore, avoid the dramatic sediment transport and ecosystem changes (e.g., nebkha dune formation) associated with transition to shrubland (Bestelmeyer et al., 2018; Okin et al., 2009; Ravi et al., 2010).

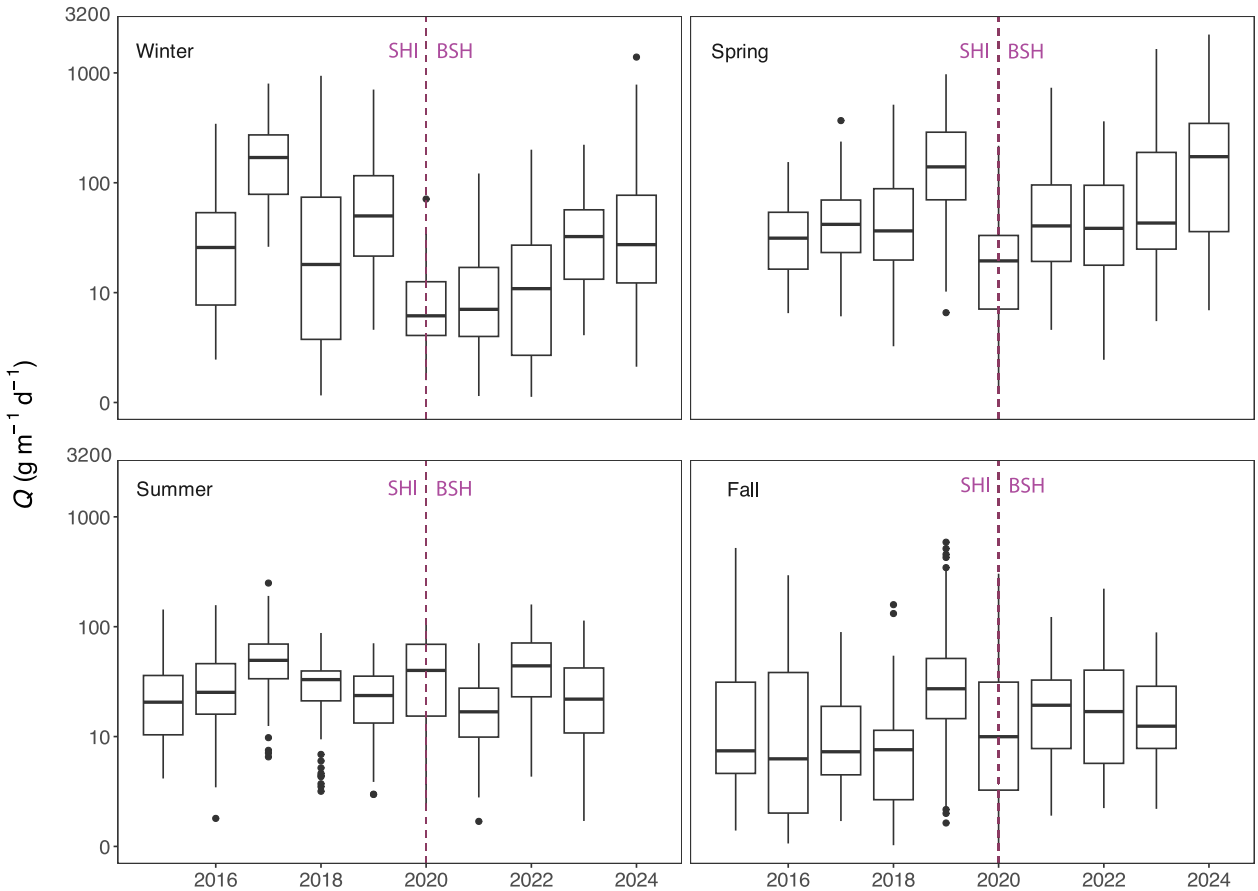

Figure 9. Seasonal horizontal sediment mass flux, Q (g m^{-1} day^{-1}) from 2015 to 2024 for the SHI site. Blue lines show trends based on Mann-Kendall trend analyses. Vertical dashed lines indicate timing of transition of the site from the shrub invaded (SHI) state to the bunchgrass/shrub (BSH) state.

The multiple orders-of-magnitude reduction in horizontal sediment flux in the grassy shrubland state (state 6), relative to the shrubland state (state 4), suggests that facilitating the recovery of perennial grasses can effectively reduce wind erosion. Importantly, although it may not always be possible to restore the species composition of historical grasslands, our results show that ecosystem processes such as sediment transport can be recovered to levels consistent with historical or more desirable ecological states. Ongoing research in the region is exploring different restoration approaches including shrub herbicide treatments (Archer & Predick, 2014), reducing bare ground connectivity using artificial structures (Peters et al., 2020), and adding manure to soils to boost nutrients where grass seedbank remains or can be added through seeding (Bethany et al., 2024).

Finally, our results confirm the utility of STMs for managing wind erosion and dust emission processes (Webb & Pierre, 2018). Shifts in the magnitude of Q at critical cover thresholds for ecological state changes indicate that the STM for our study area (Figure 2) captures key functional changes in the ecosystem. In a monitoring and assessment context, the thresholds (Figure 10) could be used as benchmarks or early warning indicators of degradation risk (Webb et al., 2024). Beyond our study area, not all ecological transitions may result in base 10 order of magnitude shifts in sediment transport rates. For example, state transitions in other Chihuahuan Desert ecosystems result in more subtle changes in vegetation cover and structure (Bestelmeyer et al., 2006; Rachal et al., 2012). Furthermore, effects of vegetation loss may be mitigated by soil surface textures, physical and biological soil crusting and high gravel cover (Bergametti & Gillette, 2010). Thus, across drylands, state transitions could result in variable changes in aeolian transport rates and/or follow a natural (≈2.718), binary (2), or other logarithmic base. Using STMs to describe wind erosion and SDS dynamics could enable managers to identify which practices may be effective for avoiding undesirable state change and accelerated wind erosion and avoid practices that are unlikely to be effective given climatic, soils, and ecological constraints.

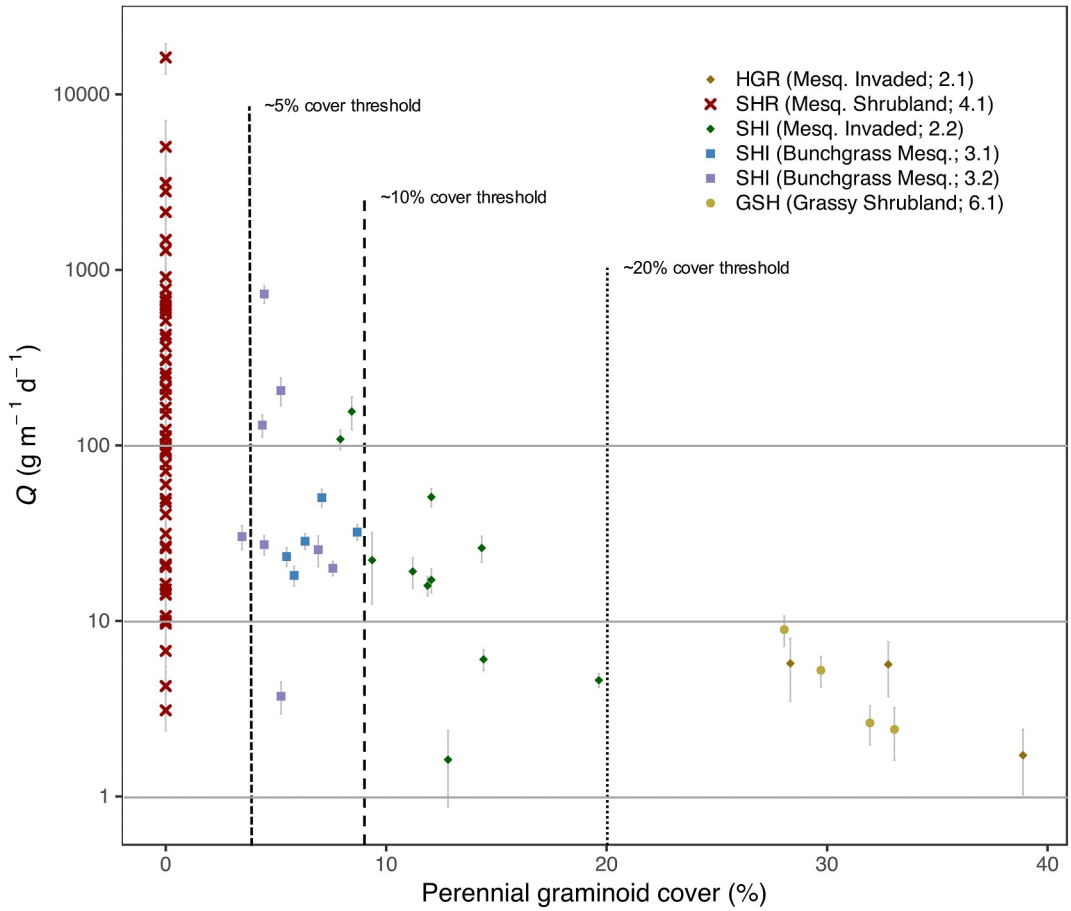

Figure 10. Relationship between Horvitz-Thomson (HT) estimator of the mean horizontal sediment flux Q (g m^{-1} d^{-1}), perennial graminoid cover (%), and ecological state. Data represent instances when transect reading coincided with sediment sampling (±2 weeks). Data for the SHR plot are shown for all sediment sampling events as no perennial grass cover was recorded at that plot in any of the transect sampling events over the study period. Error bars show the standard error of the HT mean sediment flux. Vertical dotted and dashed lines represent critical perennial grass cover thresholds for order of magnitude increases in sediment transport.

6. Conclusions

Aeolian sediment transport acts as both an endogenous and exogenous driver of ecological state change and land degradation in drylands (Payne et al., 2023). Understanding how the magnitude and spatiotemporal variability of sediment transport respond to ecosystem change is, therefore, essential for accurately assessing and mitigating wind erosion, SDS, and desertification. Using a combination of vegetation, meteorological, and sediment transport data collected across sites in the northern Chihuahuan Desert, USA, we have shown that ecological state changes can have profound effects on patterns of aeolian sediment mass flux. Crossing degradation thresholds associated with perennial grass loss and shrub encroachment, we found order-of-magnitude increases in sediment fluxes with spatiotemporal variability of sediment transport rates increasing up to four orders of magnitude within the shrubland ecological state. Crossing a restorative threshold, with grass recovery in a degraded shrubland, reduced aeolian sediment fluxes to rates consistent with those measured in the historical grassland. These changes were moderated by vegetation structural changes across ecological states. Although mesquite shrub heights were relatively consistent across ecological states, changes in the height of grasses and cover of all-plant canopy gaps >200 cm in length appeared to play a key role in determining the magnitude of sediment mass fluxes. We found that perennial grass cover of ∼20% was a critical threshold below which aeolian sediment transport rates increased exponentially within the shrub invaded state. Below ∼5% perennial grass cover, we found further order-of-magnitude increases in sediment transport that were associated with transition to shrubland. These findings

suggest aeolian transport thresholds are associated with the critical ecological thresholds for grass loss on sandy soils of our study ecosystem.

Our findings provide important new evidence for the interactions between aeolian processes and the ecological dynamics of drylands. The large positive and negative changes in magnitude and variability of sediment transport rates we observed suggest that the ecological state of land can be a primary determinant of spatiotemporal patterns of wind erosion and dust emission. This finding has important implications for the accuracy of models used to assess wind erosion and SDS, which must be sensitive to both seasonal and ecological state-related vegetation cover and structural change in order to resolve the dynamics. Accounting for ecological state change will also be important for management approaches that seek to mitigate wind erosion and SDS. Critical cover thresholds associated with ecological states and accelerated aeolian sediment transport could be used to establish monitoring benchmarks and as early warning indicators of erosion and desertification. Although grass loss resulted in profound increases in sediment transport, grass recovery, and a profound reduction in sediment transport, demonstrated that important ecosystem functions can be restored to degraded shrublands even if the historical grass species composition is not achieved. The utility of STMs for contextualizing ecological and aeolian process change together presents an opportunity for SDS source mitigation efforts to prioritize land at risk and identify practices that could be most effective given the ecological dynamics of a site.

Data Availability Statement

Data from this study can be accessed via Zenodo at doi:10.5281/zenodo.13995973 (Webb, Wheeler, et al., 2024). Data are also available through the Landscape Data Commons (https://landscapedatacommons.org). Maps were produced using ArcGIS Pro (ESRI 2023). Statistical analyses were computed in RStudio (version 2023.06.2 + 561) using the *terradactyl* (McCord et al., 2022), *spsurvey* (Dumelle et al., 2023), *stats* (R Core Team, 2024), and *EnvStats* packages (Millard, 2013). All other plots were created using the *ggplot2* R package (Wickham, 2016).

Acknowledgments
This research was a contribution of the Long-Term Agroecosystem Research (LTAR) network supported by the U.S. Department of Agriculture (USDA). We thank Laura Burkett for assistance with data collection and interpretation of ecological state classification. We thank everyone who has contributed to the Assessment, Inventory and Monitoring (AIM, Bureau of Land Management) data set. This research was supported by USDI Bureau of Land Management award #4500104319. Any use of trade, product, or firm names is for descriptive purposes only and does not imply endorsement by the US Government.

References

Achakulwisut, P., Shen, L., & Mickley, L. J. (2017). What controls springtime fine dust variability in the western United States? Investigating the 2002-2015 increase in fine dust in the U.S. Southwest. *Journal of Geophysical Research: Atmospheres*, *122*(22), 12449–12467. https://doi.org/10.1002/2017jd027208

Alvarez, L. J., Epstein, H. E., Li, J., & Okin, G. S. (2012). Aeolian process effects on vegetation communities in an arid grassland ecosystem. *Ecology and Evolution*, *2*(4), 809–821. https://doi.org/10.1002/ece3.205

Archer, S. R., & Predick, K. I. (2014). An ecosystem services perspective on brush management: Research priorities for competing land-use objectives. *Journal of Ecology*, *102*(6), 1394–1407. https://doi.org/10.1111/1365-2745.12314

Aubault, H., Webb, N. P., Strong, C. L., McTainsh, G. H., Leys, J. F., & Scanlan, J. C. (2015). Grazing impacts on the susceptibility of rangelands to wind erosion: The effects of stocking rates, stocking strategy and land condition. *Aeolian Research*, *17*, 89–99. https://doi.org/10.1016/j.aeolia.2014.12.005

Bergametti, G., & Gillette, D. A. (2010). Aeolian sediment fluxes measured over various plant/soil complexes in the Chihuahuan desert. *Journal of Geophysical Research*, *115*(F3), F03044. https://doi.org/10.1029/2009JF001543

Bestelmeyer, B. T., Okin, G. S., Duniway, M. C., Archer, S. R., Sayre, N. F., Williamson, J. C., & Herrick, J. E. (2015). Desertification, land use, and the transformation of global drylands. *Frontiers in Ecology and the Environment*, *13*(1), 28–36. https://doi.org/10.1890/140162

Bestelmeyer, B. T., Peters, D. P. C., Archer, S. R., Browning, D. M., Okin, G. S., Schooley, R. L., & Webb, N. P. (2018). The grassland-shrubland regime shift in the southwestern United States: Misconceptions and their implications for management. *BioScience*, *68*(9), 678–690. https://doi.org/10.1093/biosci/biy065

Bestelmeyer, B. T., Trujillo, D. A., Tugel, A. J., & Havstad, K. M. (2006). A multi-scale classification of vegetation dynamics in arid lands: What is the right scale for models, monitoring, and restoration. *Journal of Arid Environments*, *65*(2), 296–318. https://doi.org/10.1016/j.jaridenv.2005.06.028

Bethany, J., Kutos, S., Oliver, K., & Stricker, E. (2024). Spring manure and biosolid compost additions affect soil, vegetation, and microbial characteristic in dry rangelands. *Rangeland Ecology & Management*, *94*, 78–82. https://doi.org/10.1016/j.rama.2024.01.011

Burger, W. J., Van Pelt, R. S., Grandstaff, D. E., Wang, G., Sankey, T. T., Li, J., et al. (2023). Multi-year tracing of spatial and temporal dynamics of post-fire aeolian sediment transport using rare earth elements provide insights into grassland management. *Journal of Geophysical Research: Earth Surface*, *128*(11), e2023JF007274. https://doi.org/10.1029/2023jf007274

Christensen, E., James, D., Randall, R. M., & Bestelmeyer, B. T. (2023). Abrupt dryland transitions related to the Pacific decadal oscillation. *Ecology*, *104*(7), e4065. https://doi.org/10.1002/ecy.4065

D'Odorico, P., Bhattachan, A., Davis, K. F., Ravi, S., & Runyan, C. W. (2013). Global desertification: Drivers and feedbacks. *Advances in Water Resources*, *51*, 326–344. https://doi.org/10.1016/j.advwatres.2012.01.013

Dukes, S., Gonzales, H. B., Ravi, S., Grandstaff, D. E., Van Pelt, R. S., Li, J., et al. (2018). Quantifying postfire aeolian sediment transport using rare earth element tracers. *Journal of Geophysical Research: Biogeosciences*, *123*(1), 288–299. https://doi.org/10.1002/2017jg004284

Dumelle, M., Kincaid, T., Olsen, A. R., & Weber, M. (2023). spsurvey: Spatial sampling design and analysis in R. *Journal of Statistical Software*, *105*(3), 1–29. https://doi.org/10.18637/jss.v105.i03

Floyd, K. W., & Gill, T. E. (2011). The association of land cover with aeolian sediment production at Jornada Basin, New Mexico, USA. *Aeolian Research*, *3*(1), 55–66. https://doi.org/10.1016/j.aeolia.2011.02.002

Galloza, M. S., Webb, N. P., Bleiweiss, M., Winters, C., Herrick, J. E., & Ayers, E. (2018). Resolving dust emission responses to land cover change using an ecological land classification. *Aeolian Research*, *32*, 141–153. https://doi.org/10.1016/j.aeolia.2018.03.001

Gilbert, R. O. (1987). *Statistical methods for environmental pollution monitoring*. Wiley.

Gillette, D. A., Herrick, J. E., & Herbert, G. (2006). Wind characteristics of mesquite streets in the northern Chihuahuan Desert, New Mexico, USA. *Environmental Fluid Mechanics*, *6*(3), 241–275. https://doi.org/10.1007/s10652-005-6022-7

Gillies, J. A., Nield, J. M., & Nickling, W. G. (2014). Wind speed and sediment transport recovery in the lee of a vegetated and denuded nebkha within a nebkha dune field. *Aeolian Research*, *12*, 135–141. https://doi.org/10.1016/j.aeolia.2013.12.005

Herrick, J. E., Van Zee, J. W., McCord, S. E., Courtright, E. M., Karl, J. W., & Burkett, L. M. (2018). *Monitoring manual for grassland, shrubland, and savanna ecosystems, volume 1: Core methods, second EditionRep*. USDA-ARS Jornada Experimental Range.

Hesse, P. P., Telfer, M. W., & Farebrother, W. (2017). Complexity confers stability: Climate variability, vegetation response and sand transport on longitudinal sand dunes in Australia's deserts. *Aeolian Research*, *25*, 45–61. https://doi.org/10.1016/j.aeolia.2017.02.003

Hirsch, R. M., Slack, J. R., & Smith, R. A. (1982). Techniques of trend analysis for monthly water quality data. *Water Resources Research*, *18*(1), 107–121. https://doi.org/10.1029/wr018i001p00107

Huenneke, L. F., Anderson, J. P., Remmenga, M., & Schlesinger, W. H. (2002). Desertification alters patterns of aboveground net primary production in Chihuahuan ecosystems. *Global Change Biology*, *8*(3), 247–264. https://doi.org/10.1046/j.1365-2486.2002.00473.x

Kachergis, E., Miller, S. W., McCord, S. E., Dickard, M., Savage, S., Reynolds, L., et al. (2022). Adaptive monitoring for multiscale land management: Lessons learned from the Assessment, Inventory, and Monitoring (AIM) principles. *Rangelands*, *44*(1), 50–63. https://doi.org/10.1016/j.rala.2021.08.006

King, J., Nickling, W. G., & Gillies, J. A. (2006). Aeolian shear stress ratio measurements within mesquite-dominated landscapes of the Chihuahuan Desert, New Mexico, USA. *Geomorphology*, *82*(3–4), 229–244. https://doi.org/10.1016/j.geomorph.2006.05.004

Lambert, A., Hallar, A. G., Garcia, M., Strong, C., Andrews, E., & Hand, J. L. (2020). Dust impacts of rapid agricultural expansion on the Great Plains. *Geophysical Research Letters*, *47*(20), e2020GL090347. https://doi.org/10.1029/2020gl090347

Lancaster, N., & Baas, A. (1998). Influence of vegetation cover on sand transport by wind: Field studies at Owens Lake, California. *Earth Surface Processes and Landforms*, *23*(1), 69–82. https://doi.org/10.1002/(sici)1096-9837(199801)23:1<69::aid-esp823>3.0.co;2-g

Li, J., Okin, G. S., & Epstein, H. E. (2009). Effects of enhanced wind erosion on surface soil texture and characteristics of windblown sediments. *Journal of Geophysical Research*, *114*(G2), G02003. https://doi.org/10.1029/2008JG000903

Mahowald, N. M., & Luo, C. (2003). A less dusty future? *Geophysical Research Letters*, *30*(No. 17), 1903. https://doi.org/10.1029/2003GL017880

McCord, S. E., Brehm, J. R., Burnett, S. H., Dietrich, C., Edwards, B. L., Metz, L. J., et al. (2022). A framework and toolset for standardizing agroecosystem indicators. *Ecological Indicators*, *144*, 109511. https://doi.org/10.1016/j.ecolind.2022.109511

McCord, S. E., Webb, N. P., Bestelmeyer, B. T., Bonefont, K., Brehm, J. R., Brown, J., et al. (2023). The landscape data commons: A system for standardizing, accessing, and applying large environmental datasets for agroecosystem research and management. *Agricultural and Environmental Letters*, *8*(2), e20120. https://doi.org/10.1002/ael2.20120

Millard, S. P. (2013). *EnvStats an R package for environmental statistics* (p. 291). Springer.

Miller, M. E., Belote, R. T., Bowker, M. A., & Garman, S. L. (2011). Alternative states of a semiarid grassland ecosystem: Implications for ecosystem services. *Ecosphere*, *2*(5), 55. https://doi.org/10.1890/es11-00027.1

Mirzabaev, A., Wu, J., Evans, J., García-Oliva, F., Hussein, I. A. G., Iqbal, M. H., et al. (2019). Desertification*Rep* (pp. 249–343).

Monger, H. C. (2006). Soil development in the Jornada Basin. In K. M. Havstad, L. F. Huenneke, & W. H. Schlesinger (Eds.), *Structure and function of a Chihuahuan Desert ecosystem: The Jornada Basin long-term ecological research site* (pp. 81–106). Oxford University Press.

Munkhtsetseg, E., Shinoda, M., Ishizuka, M., Mikami, M., Kimura, R., & Nikolich, G. (2017). Anthropogenic dust emissions due to livestock trampling in a Mongolian temperate grassland. *Atmospheric Chemistry and Physics*, *17*(18), 11389–11401. https://doi.org/10.5194/acp-17-11389-2017

Niu, F., Pierce, N. A., Okin, G. S., Archer, S. R., Fischella, M. R., & Nadoum, S. (2023). Sandblasting promotes shrub encroachment in arid grasslands. *New Phytologist*, *240*(5), 1817–1829. https://doi.org/10.1111/nph.19238

Okin, G. S. (2008). A new model of wind erosion in the presence of vegetation. *Journal of Geophysical Research*, *113*(F2), F02S10. https://doi.org/10.1029/2007JF000758

Okin, G. S., Gillette, D. A., & Herrick, J. E. (2006). Multi-scale controls on and consequences of aeolian processes in landscape change in arid and semi-arid environments. *Journal of Arid Environments*, *65*(2), 253–275. https://doi.org/10.1016/j.jaridenv.2005.06.029

Okin, G. S., Parsons, A. J., Wainwright, J., Herrick, J. E., Bestelmeyer, B. T., Peters, D. P. C., & Fredrickson, E. L. (2009). Do changes in connectivity explain desertification? *BioScience*, *59*(3), 237–244. https://doi.org/10.1525/bio.2009.59.3.8

Okin, G. S., Sala, O. E., Vivioni, E. R., Zhang, J., & Bhattachan, A. (2018). The interactive role of wind and water in functioning of drylands: What does the future hold? *BioScience*, *68*(9), 670–677. https://doi.org/10.1093/biosci/biy067

Payne, S. A. R., Okin, G. S., Bhattachan, A., & Fischella, M. R. (2023). The two faces of Janus: Processes can be both exogenous forcings and endogenous feedbacks with wind as a case study. *Ecology*, *104*(4), e3998. https://doi.org/10.1002/ecy.3998

Peters, D. P. C., Okin, G. S., Herrick, J. E., Savoy, H. M., Anderson, J. P., Scroggs, S. L. P., & Zhang, J. (2020). Modifying connectivity to promote state change reversal: The importance of geomorphic context and plant–soil feedbacks. *Ecology*, *101*(9), e03069. https://doi.org/10.1002/ecy.3069

Pierre, C., Hiernaux, P., Rajot, J. L., Kergoat, L., Webb, N. P., Abdourhamane Toure, A., et al. (2021). Wind erosion respond to past and future agro-pastoral trajectories in the Sahel (Niger). *Landscape Ecology*, *37*(2), 529–550. https://doi.org/10.1007/s10980-021-01359-8

Pu, B., & Ginoux, P. (2018). Climatic factors contributing to long-term variations in surface fine dust concentration in the United States. *Atmospheric Chemistry and Physics*, *18*(6), 4201–4215. https://doi.org/10.5194/acp-18-4201-2018

Rachal, D. M., Monger, H. C., Okin, G. S., & Peters, D. P. C. (2012). Landform influences on the resistance of grasslands to shrub encroachment, northern Chihuahuan Desert, USA. *Journal of Maps*, *8*(4), 507–513. https://doi.org/10.1080/17445647.2012.727593

Ravi, S., Breshears, D. D., Huxman, T. E., & D'Odorico, P. (2010). Land degradation in drylands: Interactions among hydrologic-aeolian erosion and vegetation dynamics. *Geomorphology*, *116*(3–4), 236–245. https://doi.org/10.1016/j.geomorph.2009.11.023

R Core Team. (2024). *R: A language and environment for statistical computing*. R Foundation for Statistical Computing. Retrieved from https://www.R-project.org

Robinson, M. C., & Ardon-Dryer, K. (2024). Characterization of 21 years of dust events across four West Texas regions. *Aeolian Research*, *67–69*, 100930. https://doi.org/10.1016/j.aeolia.2024.100930

Sankey, J. B., Germino, M. J., & Glenn, N. F. (2012). Dust supply varies with sagebrush microsites and time since burning in experimental erosion events. *Journal of Geophysical Research*, *117*(G1), G01013. https://doi.org/10.1029/2011JG001724

Sasaki, T., Koyama, A., & Okuro, T. (2018). Coupling structural and functional thresholds for vegetation changes on a Mongolian shrubland. *Ecological Indicators*, *93*, 1264–1275. https://doi.org/10.1016/j.ecolind.2018.06.032

Shao, Y., Wyrwoll, K.-H., Chappell, A., Huang, J., Lin, Z., McTainsh, G. H., et al. (2011). Dust cycle: An emerging core theme in Earth system science. *Aeolian Research*, *2*(4), 181–204. https://doi.org/10.1016/j.aeolia.2011.02.001

Tegen, I., Werner, M., Harrison, S. P., & Kohfeld, K. E. (2004). Relative importance of climate and land use in determining present and future global soil dust emission. *Geophysical Research Letters*, *31*(5), L05105. https://doi.org/10.01029/02003GL0191216

Treminio, R. S., Webb, N. P., Edwards, B. L., Faist, A. M., Newingham, B., & Kachergis, E. (2024). Spatial patterns and controls on wind erosion in the Great Basin. *Journal of Geophysical Research: Biogeosciences*, *129*(1), e2023JG007792. https://doi.org/10.1029/2023jg007792

UNCCD. (2022). Sand and dust storms compendium: Information and guidance on assessing and addressing the Risks*Rep* (p. 345).

Wainwright, J. (2006). Climate and climatological variations in the Jornada Basin. In K. M. Havstad, L. F. Huenneke, & W. H. Schlesinger (Eds.), *Structure and function of a Chihuahuan Desert ecosystem: The Jornada Basin long-term ecological research site* (pp. 44–80). Oxford University Press.

Webb, N. P., Chappell, A., Edwards, B. L., McCord, S. E., Van Zee, J. W., Cooper, B. F., et al. (2019). Reducing sampling uncertainty in aeolian research to improve change detection. *Journal of Geophysical Research: Earth Surface*, *124*(6), 1366–1377. https://doi.org/10.1029/2019jf005042

Webb, N. P., Edwards, B. L., Heller, A., McCord, S. E., Schallner, J. W., Treminio, R. S., et al. (2024). Establishing quantitative benchmarks for soil erosion and ecological monitoring, assessment, and management. *Ecological Indicators*, *159*, 111661. https://doi.org/10.1016/j.ecolind.2024.111661

Webb, N. P., Herrick, J. E., & Duniway, M. C. (2014). Ecological site-based assessments of wind and water erosion: Informing accelerated soil erosion management in rangelands. *Ecological Applications*, *24*(6), 1405–1420. https://doi.org/10.1890/13-1175.1

Webb, N. P., Herrick, J. E., Hugenholtz, C. H., Zobeck, T. M., & Okin, G. S. (2015). *Standard methods for wind erosion research and model development: Protocol for the national wind erosion research network*. USDA-ARS Jornada Experimental Range.

Webb, N. P., Herrick, J. E., Van Zee, J. W., Courtright, E. M., Hugenholtz, C. H., Zobeck, T. M., et al. (2016). The National Wind Erosion Research Network Building a standardized long-term data resource for aeolian research, modeling and land management. *Aeolian Research*, *22*, 23–36. https://doi.org/10.1016/j.aeolia.2016.05.005

Webb, N. P., Kachergis, E., Miller, S. W., McCord, S. E., Bestelmeyer, B. T., Brown, J. R., et al. (2020). Indicators and benchmarks for wind erosion monitoring, assessment and management. *Ecological Indicators*, *110*, 105881. https://doi.org/10.1016/j.ecolind.2019.105881

Webb, N. P., LeGrand, S. L., Cooper, B. F., Courtright, E. M., Edwards, B. L., Felt, C., et al. (2021). Size distribution of mineral dust emissions from sparsely vegetated and supply-limited dryland soils. *Journal of Geophysical Research: Atmospheres*, *126*(22), e2021JD035478. https://doi.org/10.1029/2021jd035478

Webb, N. P., Marshall, N. A., Stringer, L. C., Reed, M. S., Chappell, A., & Herrick, J. E. (2017). Land degradation and climate change: Building climate resilience in agriculture. *Frontiers in Ecology and the Environment*, *15*(8), 450–459. https://doi.org/10.1002/fee.1530

Webb, N. P., McCord, S. E., Edwards, B. L., Herrick, J. E., Kachergis, E., Okin, G. S., & Van Zee, J. W. (2021). Vegetation canopy gap size and height: Critical indicators for wind erosion monitoring and management. *Rangeland Ecology & Management*, *76*, 78–83. https://doi.org/10.1016/j.rama.2021.02.003

Webb, N. P., Okin, G. S., & Brown, S. (2014). The effect of roughness elements on wind erosion: The importance of surface shear stress distribution. *Journal of Geophysical Research: Atmospheres*, *119*(10), 6066–6084. https://doi.org/10.1002/2014jd021491

Webb, N. P., & Pierre, C. (2018). Quantifying anthropogenic dust emissions. *Earth's Future*, *6*(2), 286–295. https://doi.org/10.1002/2017ef000766

Webb, N. P., Wheeler, B. E., Edwards, B. L., Schallner, J. W., Macanowicz, N., & Van Zee, J. W. (2024). Data used for the analysis "Magnitude shifts in aeolian sediment transport associated with degradation and restoration thresholds in drylands" (version 1.0). *Zenodo*. [Dataset]. https://doi.org/10.5281/zenodo.13995973

Wickham, H. (2016). *Elegant graphics for data analysis*. Springer-Verlag.

Wiggs, G. F. S., Thomas, D. S. G., Bullard, J. E., & Livingstone, I. (1995). Dune mobility and vegetation cover in the southwest Kalahari Desert. *Earth Surface Processes and Landforms*, *20*(6), 515–529. https://doi.org/10.1002/esp.3290200604

Wojcikiewicz, R. R. K., Webb, N. P., Edwards, B. L., Van Zee, J. W., Courtright, E. M., Cooper, B. F., & Hanan, N. P. (2023). Aeolian sediment transport responses to vegetation cover change: Effects of sampling error on model uncertainty. *Journal of Geophysical Research: Earth Surface*, *128*(12), e2023JF007319. https://doi.org/10.1029/2023jf007319

Woodward, S., Roberts, D. L., & Betts, R. A. (2005). A simulation of the effect of climate change-induced desertification on mineral dust aerosol. *Geophysical Research Letters*, *32*(18), L18810. https://doi.org/10.1029/2005gl023482

Yu, C. L., Li, J., Karl, M. G., & Krueger, T. J. (2020). Obtaining a balanced area sample for the Bureau of land management rangeland survey. *Journal of Agricultural, Biological, and Environmental Statistics*, *25*(2), 250–275. https://doi.org/10.1007/s13253-020-00392-5

Zheng, M., Song, J., Ru, J., Zhou, Z., Zhong, M., Jiang, L., et al. (2021). Effects of grazing, wind erosion, and dust deposition on plant community composition and structure in a temperate steppe. *Ecosystems*, *24*(2), 403–420. https://doi.org/10.1007/s10021-020-00526-3

Ziegler, N. P., Webb, N. P., Gillies, J. A., Edwards, B. L., Nikolich, G., Van Zee, J. W., et al. (2023). Plant phenology drives seasonal changes in shear stress partitioning in a semi-arid rangeland. *Agricultural and Forest Meteorology*, *330*, 109295. https://doi.org/10.1016/j.agrformet.2022.109295